POLITECNICO DI TORINO

Corso di Laurea Magistrale

in Ingegneria Meccanica

Tesi di Laurea Magistrale

Frequency domain models for active suspension controller design

Relatore

Alessandro Vigliani

Candidato

Alessandro Percolla

Corelatori

Aldo Sorniotti

Enrico Galvagno

Anno Accademico 2018/19

Table of contents

Abstract

In the past years a lot of different chassis control system have been developed in order to improve handling performance, ride comfort and safety of the vehicle. These chassis control systems are based mainly on the active control of the steering system, the traction/braking system and the suspensions. Depending on the riding conditions one of these systems can be more effective than the others, so it difficult to choose the best compromise for al the possible scenarios. For this reason, most of the new studies on this topic are focusing on the integration of all of the available control system to obtain and Integrated Chassis Control (ICC) system able to improve the vehicle performances in a wide range of operation conditions. In this context, being able to formulate the control law for the ICC is the key to achieve the expected results. In this thesis a model-based procedure for the design of the controllers is presented taking as an example the synthesis of an anti-roll moment distribution controller for yaw rate tracking. The model used in this case is a simple model in which only 3 degrees of freedom are taken into account, but in order to apply the model-based approach to a wide range of active systems like dynamic lift or pitch control, a more advanced vehicle model is needed. For this purpose, a full vehicle model with 6 degrees of freedom with active suspensions and which takes the suspension kinematics into account is presented. The response of the newly developed model is then compared to that of a validated vehicle model by simulating different manoeuvres. Finally, the procedure to linearise the model is presented to obtain the state space formulation which can be used, by using the model-based approach, to synthetize a variety of controllers and thus to obtain the control laws needed for the implementation of an Integrated Chassis Control.

1 Introduction

In the last years many studies have been focused on the design of automatic control devices for road vehicles which are able to perform autonomously different control functions that usually are a support for the driver, but, in some cases, they can even replace the driver action. As said in "*The automotive chassis: volume 2"* (2008) by the author *G. Genta,* the most actively studied control system are:

- Engine control systems
- Longitudinal slip control in traction (ASR, Anti Spin Regulator)
- Longitudinal slip control in braking (ABS, Antilock Braking System)
- Vehicle dynamics control systems, (VDC, Vehicle Dynamic Control, ESP, Enhanced Stability Program, DSC, Dynamics Stability Control)
- Suspension control systems (semi-active and active suspensions) that are capable of adapt the suspension characteristics to the type and conditions of the road
- Active steer control
- Electric braking
- Servo controlled gearbox and clutch

In particular, the vehicle dynamics control systems are implemented in order to achieve improved vehicle performance and safety in limit conditions. Usually these systems act by generating a yaw torque capable of modifying the vehicle behaviour. This yaw torque is often produced by differentially braking or differentially driving (torque vectoring) the wheels of the same axle. When these systems are activated, the driver can control the trajectory normally through the steering wheel and the control device tries to modify the vehicle behaviour, by applying the yaw torque, to obtain the response required by the steering input of the driver.

Another way to control the lateral dynamics of the vehicle it by actively modifying the balance of the lateral forces exerted by the tires. This can be obtained by means of active anti-roll bars that can be controlled to modify the lateral load distribution between he front and rear axle of the vehicle, thus

controlling the lateral force generated by the two axles. This kind of system has been studied by many authors, and in the next section this topic will be discussed more in details.

1.1 Anti-Roll moment distribution control (Force Vectoring)

It is possible to enhance the cornering response of a vehicle by means of an active suspension system, which allows to vary the lateral load transfer distribution between the front and rear axles, e.g., to enable higher levels of lateral acceleration during cornering and to mitigate vehicle understeering in quasi-steady-state conditions, and to increase yaw and sideslip damping in transient conditions. Lateral load transfer produces a variation of the axle lateral force and in particular its distribution, between the front and rear axle, affects the cornering response of the vehicle. In [1]-[2] the authors analyse this effect by observing the resulting axle lateral forces from fully nonlinear tyre models under different conditions.

Clover et al. [3] examine how the lateral load transfer distribution influences the understeering characteristics of the vehicle, via computer simulation. The analysis is carried out for different values of the vehicle lateral acceleration and the results show that, in limit handling conditions, the distribution of lateral load transfer is indeed very influential on the understeer characteristics of the vehicle.

Electronically controllable suspension systems have been already used for tracking a reference yaw rate and shaping the understeer characteristics of a vehicle and some results are presented in [4]-[7]. Moreover, Shim et al. [6] addresses the effectiveness of active suspension control over lateral and longitudinal vehicle dynamics obtained by modulating the normal load for each wheel. The control of normal forces is assessed on several scenarios including split μ and cornering over bumpy roads. The results show improved vehicle handling when normal force control is active. In addition, the authors investigate the power requirements of the active suspension actuators. Varnhagen et al. [8] propose an active suspension system to improve the vehicle lateral dynamics by controlling the wheel vertical forces, but with negligible effects on the chassis heave-pitch-roll dynamics. Yamamoto [9] analyses the effect of different active control systems (including vertical load control) on yaw and lateral motion of the vehicle in both the linear and nonlinear range of the tyre forces. The results confirm the improvement in vehicle handling given by the use of active systems. Finally, Elbeheiry et al. [7] propose an integration between active front steering and active roll moment control systems in order to enhance vehicle controllability in case of emergency manoeuvres.

1.2 Thesis content

The content of this thesis can be summarised in three main parts:

- Section 2 will present a procedure based on the model-based design approach to design the controller for active anti-roll bars (force vectoring)
- Section 3 will present the procedure used to obtain a novel vehicle model in which the suspensions kinematic is taken into account and an active suspension system is implemented. After the model definition, a procedure to linearise it for controller design purpose will be described.
- Section 4 will present the conclusions and the future developments of this study

2 Model based controller design: anti-roll moment distribution controllers for yaw rate tracking

In the context of anti-roll moment distribution active control, a model-based approach can be used in order to synthesize the final controller for the vehicle. The model-based approach involves the creation of a vehicle model, capable of representing faithfully the yaw dynamics, which is then linearised to be used as the plant of the system. The plant of the system consists in a transfer function between the input given to the system and the output needed to create the feedback loop, ones this transfer function is obtained it's possible to apply a simple PI controller and tune it via an optimization routine built in MATLAB environment, thus obtaining the optimal gains for the controller.

In this context it is essential to formulate mathematical vehicle models that correctly approximate the tyre behaviour in cornering under different vertical loading conditions and that can therefore be used for control design purpose. Furukawa et al. [1] assess the effectiveness of direct yaw moment control and active steering in case of high lateral acceleration conditions and state that: "taking the nonlinearity of tyres and vehicle dynamics into consideration is essential for introducing the control law for the chassis controls". In particular, their study shows how the tyre nonlinearities can heavily influence the generation of the stabilising yaw moment, and therefore why it is of the essence to consider them in the controller

design stage. In addition to that, the study recognises the treatment of nonlinear tyre characteristics as the main issue in the area of chassis controls.

Regarding model-based suspension control design, Jialing et al. [2] state that due to the high level of nonlinearity in the effect of the lateral load transfer on the lateral dynamics of the vehicle, it is necessary to formulate mathematical models that, although approximated, are still able to catch the fundamental effects of load transfer. Various approaches have been proposed in the past years in the literature. In [3] [4] [5] the authors use the commonly adopted parabolic relationship between the axle cornering stiffness and lateral load transfer. In particular, Chu et al. [5] investigate the relationship between the nonlinear cornering stiffness, tyre coefficients, front-to-rear roll stiffness ratio and lateral load transfer. Similarly, in [6] Bodie et al. present a formulation for the axle cornering stiffness which includes a quadratic relationship with the axle lateral load transfer. Badji et al. [7] propose a cubic formulation of the lateral force via a Taylor series expansion of the Pacejka magic formula [8], while Lakehal-Ayat et al. [9] adopt a nonlinear single-track vehicle model including a combination between a parabolic formulation and a simplified Pacejka Magic Formula to describe the axle lateral force, and use this model for the design of a yaw rate tracking controller. In [10] Cho et al. compute the cornering stiffness to be used in the tyre model of a single-track vehicle model as a weighted function of two different cornering stiffness values corresponding to specific vehicle cornering conditions (namely agility and manoeuvrability cornering stiffness). Similarly, Shin et al. [11] propose a linearised model formulation for state estimation purpose in which the cornering stiffness value is updated depending on the operating conditions of the vehicle.

This section presents a linearised model for control design specifically applied to the design of front-to-total anti-roll moment distribution controllers for yaw rate tracking. The control strategy implies a feed forward contribution that is derived using a quasi-static model whereas the feedback part is based on a PI (proportional-integral controller) that is designed using the presented vehicle model. The controller is then tested in simulation using a validated nonlinear vehicle model of an SUV (Sport Utility Vehicle).

2.1 Model description

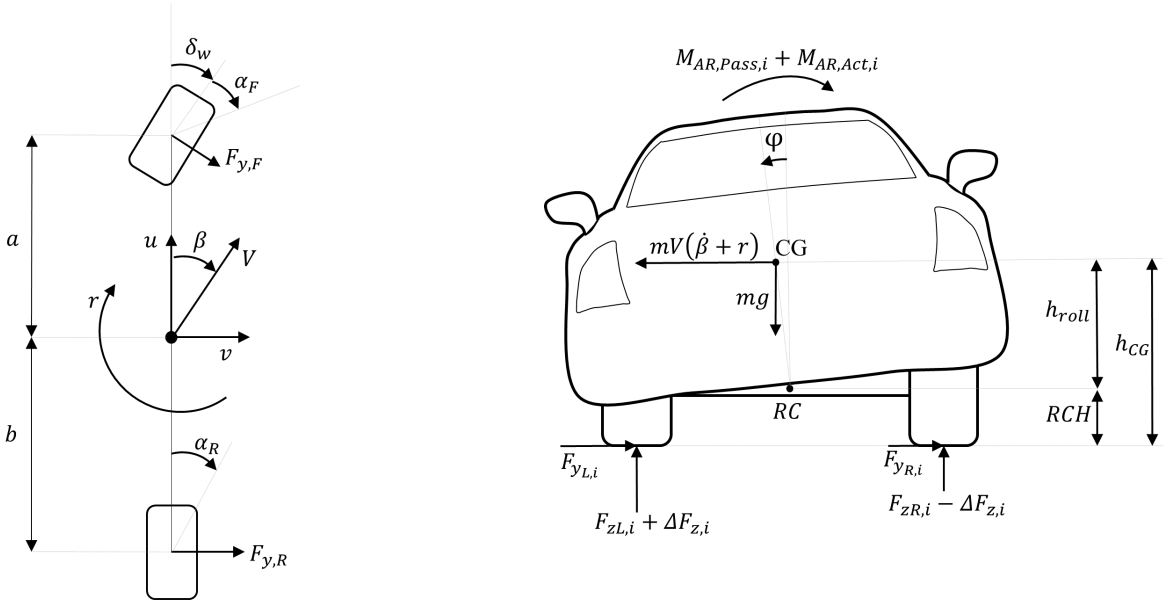

Figure 1. Top view of the single-track model and rear view of the vehicle with indication of the sign conventions, main variables and constants

In this model the roll moment balance equation is added to the force balance equations of the classic bicycle model resulting in the following system:

$$\begin{cases} mV(\dot{\beta} + r) = F_{y,F} + F_{y,R} \\ I_z \dot{r} = F_{y,F} a - F_{y,R} b + M_{z,Ext} \\ I_x \ddot{\varphi} = mV(\dot{\beta} + r) h_{\mathrm{CG}} + mg h_{\mathrm{CG}} \varphi - M_{AR,Pass,F} - M_{AR,Pass,R} - M_{AR,Act,F} - M_{AR,Act,I} \end{cases} \quad (1)$$

where m is the mass of the vehicle, V is the vehicle speed, r is the vehicle yaw rate, $\dot{\beta}$ is the time derivative of the sideslip angle at the centre of gravity of the vehicle, $F_{y,F}$ and $F_{y,R}$ are the lateral forces at the front and rear axles, I_z is the yaw moment of inertia, $\dot{r}$ is the yaw acceleration, a is the front semi-wheelbase, b is the rear semi-wheelbase, $M_{z,Ext}$ represents the external contributions of the yaw moment, I_x is the roll moment of inertia, $\ddot{\varphi}$ is the roll acceleration, h_{CG} is the centre of gravity height, g is the gravity acceleration, φ is the roll angle, $M_{AR,Pass,F}$ and $M_{AR,Pass,R}$ are the passive contributions of the anti-roll

moments on the front and rear axles, $M_{AR,Act,F}$ and $M_{AR,Act,R}$ are the active contributions of the anti-roll moment.

The passive contributions of the anti-roll moment are described by:

$$\begin{aligned} M_{AR,Pass,F} &= K_F\varphi + D_F\dot{\varphi} \\ M_{AR,Pass,R} &= K_R\varphi + D_R\dot{\varphi} \end{aligned} \tag{2}$$

where K_F and K_R are the roll stiffnesses on the front and rear axles, D_F and D_R are the roll damping coefficients on the front and rear axles and $\dot{\varphi}$ is the roll rate.

The active contribution of the anti-roll moments is expressed as function of the lateral acceleration as follows:

$$\begin{aligned} M_{AR,Act,F} &= mV\big(\dot{\beta}+r\big)\left(\frac{b}{a+b}RCH + f(h_{CG} - RCH\ \right)k \\ M_{AR,Act,R} &= mV\big(\dot{\beta}+r\big)\left(\frac{a}{a+b}RCH + (1-f\ (h_{CG} - RCH\ \right)k \end{aligned} \tag{3}$$

where the term $V\big(\dot{\beta}+r\big)$ represents the lateral acceleration a_y, k is a gain that indicates the level of activation of the controller. The term RCH represents the height of the roll center from the ground. The term f is the control variable and it is defined as the ratio between the active front anti-roll moment and the total active anti-roll moment:

$$\begin{aligned} f &= \frac{M_{AR,Act,F}}{M_{AR,Act,Tot}} \\ M_{AR,Act,Tot} &= M_{AR,Act,F} + M_{AR,Act,R} \end{aligned} \tag{4}$$

For the design of the controller it is supposed that $h_{roll} = h_{CG}$ (Figure 1), so that RCH is zero.

By making these assumption Equation (1) can be re-written as:

$$\begin{aligned} M_{AR,Act,F} &\approx mV\big(\dot{\beta}+r\big)h_{CG}fk \\ M_{AR,Act,R} &\approx mV\big(\dot{\beta}+r\big)h_{CG}(1-f\ k \end{aligned} \tag{5}$$

The front and rear sideslip angles are:

$$\alpha_F = \beta + \frac{a}{V} r - \delta_w$$
$$\alpha_R = \beta - \frac{b}{V} r \tag{6}$$

where δ_w is the steering angle. The lateral load transfer on the i-th axle is then calculated as:

$$\Delta F_{z,i} = \frac{M_{AR,Act,i} + M_{AR,Pass,i}}{t_i} \tag{7}$$

where t_i is the track width of the i-th axle.

In this model a linearised model is realised so that it expresses the relationship between lateral axle force $F_{y,i}$, sideslip angle α_i and lateral load transfer ΔF_z, for the i-th axle. The linearisation point is defined by the value of the lateral load transfer $\Delta F_{z,i,0}$ and sideslip angle $\alpha_{i,0}$, as well as the corresponding axle lateral force $F_{y,i,lin,0}$ and axle cornering stiffness $C_{i,0}$. The axle lateral force $F_{y,i}$ can be expressed as linear function of the sideslip angle α_i:

$$F_{y,i} \approx F_{y,i,lin} + C_i(\alpha_i - \alpha_{i,0}) \tag{8}$$

The values of $F_{y,i}$ and C_i can be expressed as functions of the lateral load transfer $\Delta F_{z,i}$, consequently, adopting a first order Taylor series expansion, the following linear equations are obtained:

$$C_i \approx C_{i,0} + C'_{i,0}(\Delta F_{z,i} - \Delta F_{z,i,0})$$
$$F_{y,i,lin} = F_{y,i,lin,0} + F'_{y,i,lin,0}(\Delta F_{z,i} - \Delta F_{z,i,0}) \tag{9}$$

Where $C'_{i,0}$ and $F'_{y,i,lin,0}$ are the axle cornering stiffness and lateral axle force gradients with respect to load transfer. Combining Equation (8) and Equation (9) the final linearised model is represented by:

$$F_{y,i} \approx F_{y,i,lin,0} + F'_{y,i,lin,0}(\Delta F_{z,i} - \Delta F_{z,i,0}) + (\alpha_i - \alpha_{i,0})[C_{i,0} + C'_{i,0}(\Delta F_{z,i} - \Delta F_{z,i,0}\ ] \tag{10}$$

Substituting Equation (5), Equation (6) and Equation (7) in Equation (10) the front and rear axle lateral forces become:

$$F_{y,F} \approx F_{y,F,lin,0} + F'_{y,F,lin,0}\left(\frac{fh_{CG}mV(\dot{\beta}+r)k + K_F\varphi + D_F\dot{\varphi}}{t_F} - \Delta F_{z,F,0}\right) + \left(\beta + \frac{a}{V}r - \delta_w - \alpha_{F,0}\right)\left[C_{F,0} + C'_{F,0}\left(\frac{fh_{CG}mV(\dot{\beta}+r)k + K_F\varphi + D_F\dot{\varphi}}{t_F} - \Delta F_{z,F,0}\right)\right] \tag{11}$$

$$F_{y,R} \approx F_{y,R,lin,0} + F'_{y,R,lin,0}\left(\frac{(1-f\ h_{CG}mV(\dot{\beta}+r)k + K_R\varphi + D_R\dot{\varphi}}{t_R} - \Delta F_{z,R,0}\right) + \left(\beta - \frac{b}{V}r - \alpha_{R,0}\right)\left[C_{R,0} + C'_{R,0}\left(\frac{(1-f\ h_{CG}mV(\dot{\beta}+r)k + K_R\varphi + D_R\dot{\varphi}}{t_R} - \Delta F_{z,R,0}\right)\right] \tag{12}$$

By replacing Equation (2) and (Equation (5) in the roll equation in Equation (1), dividing for I_x and rearranging it holds that:

$$\ddot{\varphi} = mV(\dot{\beta}+r)(1-k\ \frac{h_{CG}}{I_x} + mg\frac{h_{CG}}{I_x}\varphi - \frac{K_F\varphi + D_F\dot{\varphi} + K_R\varphi + D_R\dot{\varphi}}{I_x} \tag{13}$$

By substituting Equation (11) and Equation (12) in the system Equation (1), the final equations of the model are obtained. The states of the system finally are: β, r, φ and $\dot{\varphi}$ while f and $M_{z,Ext}$ represent the inputs. The variable δ_w is not directly influenced by the controller, so it is considered as a disturbance of the system.

2.2 Linearisation

The state x, the input u and disturbance d vectors are defined as follows:

$$x = \begin{bmatrix}\beta\\ r\\ \varphi\\ \dot{\varphi}\end{bmatrix}, \qquad u = \begin{bmatrix}f\\ M_{z,ext}\end{bmatrix}, \qquad d = [\delta_w] \tag{14}$$

The variables are linearised resulting in the following:

$$x = x_0 + \delta x \qquad \dot{x} = \dot{x}_0 + \delta\dot{x} \qquad u = u_0 + \delta u \qquad d = d_0 + \delta d \tag{15}$$

where x_0, $\dot{x}_0$ and u_0 are the equilibrium points.

By substituting (26) in the previously defined differential equations, the system becomes:

$$\begin{cases} \dot{\beta}_0 + \delta\dot{\beta} = F(\beta_0 + \delta\beta, r_0 + \delta r, \varphi_0 + \delta\varphi, \dot{\varphi}_0 + \delta\dot{\varphi}, f_0 + \delta f, \delta_{w,0} + \delta\delta_w, M_{z,Ext,0} + \delta M_{z,Ext}) \\ \dot{r}_0 + \delta\dot{r} = G(\beta_0 + \delta\beta, r_0 + \delta r, \varphi_0 + \delta\varphi, \dot{\varphi}_0 + \delta\dot{\varphi}, f_0 + \delta f, \delta_{w,0} + \delta\delta_w, M_{z,Ext,0} + \delta M_{z,Ext}) \\ \dot{\varphi}_0 + \delta\dot{\varphi} = B(\beta_0 + \delta\beta, r_0 + \delta r, \varphi_0 + \delta\varphi, \dot{\varphi}_0 + \delta\dot{\varphi}, f_0 + \delta f, \delta_{w,0} + \delta\delta_w, M_{z,Ext,0} + \delta M_{z,Ext}) \\ \ddot{\varphi}_0 + \delta\ddot{\varphi} = H(\beta_0 + \delta\beta, r_0 + \delta r, \varphi_0 + \delta\varphi, \dot{\varphi}_0 + \delta\dot{\varphi}, f_0 + \delta f, \delta_{w,0} + \delta\delta_w, M_{z,Ext,0} + \delta M_{z,Ext}) \end{cases} \tag{16}$$

where F, G and H are the three initial differential equations and B is a trivial equation (i.e. $\frac{d}{dt}\varphi = \dot{\varphi}$) to obtain a square state matrix A.

The linearised equations are now in the following general form:

$$\begin{aligned} \delta\dot{\beta} &= \sum_{j=1}^{n} \frac{\partial F}{\partial \delta x_j}\bigg|_{\substack{\delta x=0 \\ \delta u=0 \\ \delta d=0}} \delta x_j + \sum_{k=1}^{m} \frac{\partial F}{\partial \delta u_k}\bigg|_{\substack{\delta x=0 \\ \delta u=0 \\ \delta d=0}} \delta u_k + \sum_{i=1}^{p} \frac{\partial F}{\partial \delta d_i}\bigg|_{\substack{\delta x=0 \\ \delta u=0 \\ \delta d=0}} \delta d_i \\ \delta\dot{r} &= \sum_{j=1}^{n} \frac{\partial G}{\partial \delta x_j}\bigg|_{\substack{\delta x=0 \\ \delta u=0 \\ \delta d=0}} \delta x_j + \sum_{k=1}^{m} \frac{\partial G}{\partial \delta u_k}\bigg|_{\substack{\delta x=0 \\ \delta u=0 \\ \delta d=0}} \delta u_k + \sum_{i=1}^{p} \frac{\partial G}{\partial \delta d_i}\bigg|_{\substack{\delta x=0 \\ \delta u=0 \\ \delta d=0}} \delta d_i \\ \delta\dot{\varphi} &= \sum_{j=1}^{n} \frac{\partial B}{\partial \delta x_j}\bigg|_{\substack{\delta x=0 \\ \delta u=0 \\ \delta d=0}} \delta x_j + \sum_{k=1}^{m} \frac{\partial B}{\partial \delta u_k}\bigg|_{\substack{\delta x=0 \\ \delta u=0 \\ \delta d=0}} \delta u_k + \sum_{i=1}^{p} \frac{\partial B}{\partial \delta d_i}\bigg|_{\substack{\delta x=0 \\ \delta u=0 \\ \delta d=0}} \delta d_i \\ \delta\ddot{\varphi} &= \sum_{j=1}^{n} \frac{\partial H}{\partial \delta x_j}\bigg|_{\substack{\delta x=0 \\ \delta u=0 \\ \delta d=0}} \delta x_j + \sum_{k=1}^{m} \frac{\partial H}{\partial \delta u_k}\bigg|_{\substack{\delta x=0 \\ \delta u=0 \\ \delta d=0}} \delta u_k + \sum_{i=1}^{p} \frac{\partial H}{\partial \delta d_i}\bigg|_{\substack{\delta x=0 \\ \delta u=0 \\ \delta d=0}} \delta d_i \end{aligned} \tag{17}$$

where x_j, u_k and d_i represent the j-th, the k-th, and the i-th element of the state vector, input vector and disturbance vector, respectively. n, m and p are the dimensions of the state vector, input vector and disturbance vector.

Considering Equation (15), the time derivative of the right-hand-side of the state vector equation $x_0 + \delta x$ can be written in the Taylor series expansion form:

$$\dot{x}_0 + \delta\dot{x} = \; Q(x_0, u_0, d_0 \; + \frac{\partial Q}{\partial x}\bigg|_{\substack{\delta x=0 \\ \delta u=0 \\ \delta d=0}} \delta x + \frac{\partial Q}{\partial u}\bigg|_{\substack{\delta x=0 \\ \delta u=0 \\ \delta d=0}} \delta u + \frac{\partial Q}{\partial d}\bigg|_{\substack{\delta x=0 \\ \delta u=0 \\ \delta d=0}} \delta d \tag{18}$$

where Q is the generic function considered.

Since:

$$\dot{x}_0 = \ Q(x_0, u_0, d_0 \tag{19}$$

it is possible to write the system of linearised equations in a matrix form:

$$\delta\dot{x} = A\delta x + B\delta u + E\delta d \tag{31}$$

where A, B and E are the state, input and disturbance Jacobian matrices.

2.2.1 Selection of the linearisation points

The constant terms found into the Jacobian matrices derived from the vehicle models are: i) the constants of the models and ii) the linearisation points. The latter are calculated by means of the quasi-static model in [12] and [13]. Table I shows the main vehicle parameters used for this operation.

TABLE I. MAIN VEHICLE PARAMETERS

Symbols	Description	Quantity
m	Vehicle mass	2530 kg
a	Front semi-wheelbase	1.559 m
b	Rear semi-wheelbase	1.374 m
h_{CG}	Height of the centre of gravity	0.72 m
t_F	Front track width	1.676 m
t_R	Rear track width	1.742 m
K_F	Front roll stiffness	58589 N/rad
K_R	Rear roll stiffness	49900 N/rad
D_F	Front roll damping	5730 Nm s/rad
D_R	Rear roll damping	5730 Nm s/rad
I_x	Roll inertia	560.7 kg m^2
I_z	Yaw inertia	3500 kg m^2

In particular, the following constants are selected: $\alpha_{i,0}$, $\Delta F_{z,i,0}$, φ_0, β_0, r_0, $\delta_{w,0}$, f_0, $F'_{y,i,0}$ and $C'_{i,0}$. All the terms with the index "i" are related to the i-th axle; $F'_{y,i,0}$ and $C'_{i,0}$ are the derivatives of the lateral force and the cornering stiffness on the i-th axle, respectively, calculated in the linearisation point. Different values of lateral accelerations (i.e., 3 m/s^2, 6 m/s^2 and 9 m/s^2) are considered together with a vehicle speed of 100 km/h. The term $F_{y,i,0}$ is calculated through an interpolation procedure using the Pacejka magic formula for the three linearisation conditions (i.e. different lateral accelerations).

As expected, if the constants calculated above were taken directly form a quasi-static model and imposed in the analysed model, this would generate inconsistency in the linearisation points due to the different level of fidelity of the model respect to the quasi-static one. In particular the dynamic response of the dynamic model can differ from the quasi-static model by imposing the same values for yaw rate and front-to-total anti-roll moment ratio found with the latter. The following generic procedure was used to tackle this issue.

Starting from Equation (16), a steady state condition is imposed resulting in:

$$\begin{cases} 0 = F(\beta_0 + \delta\beta, r_0 + \delta r, \varphi_0 + \delta\varphi, \dot{\varphi}_0 + \delta\dot{\varphi}, \delta_{w,0} + \delta\delta_w, f_0 + \delta f, M_{z,Ext,0} + \delta M_{z,Ext}) \\ 0 = G(\beta_0 + \delta\beta, r_0 + \delta r, \varphi_0 + \delta\varphi, \dot{\varphi}_0 + \delta\dot{\varphi}, \delta_{w,0} + \delta\delta_w, f_0 + \delta f, M_{z,Ext,0} + \delta M_{z,Ext}) \\ 0 = B(\beta_0 + \delta\beta, r_0 + \delta r, \varphi_0 + \delta\varphi, \dot{\varphi}_0 + \delta\dot{\varphi}, \delta_{w,0} + \delta\delta_w, f_0 + \delta f, M_{z,Ext,0} + \delta M_{z,Ext}) \\ 0 = H(\beta_0 + \delta\beta, r_0 + \delta r, \varphi_0 + \delta\varphi, \dot{\varphi}_0 + \delta\dot{\varphi}, \delta_{w,0} + \delta\delta_w, f_0 + \delta f, M_{z,Ext,0} + \delta M_{z,Ext}) \end{cases} \tag{32}$$

At this point f_0 and r_0 are imposed equal to the quasi-static model values, whereas β_0, φ_0 and $\delta_{w,0}$ are calculated solving the system of three equations and three unknowns. This was achieved using the symbolic algebra software Maple.

2.3 Frequency response

Once the model has been linearised it is possible to obtain the frequency response of the plant ($\delta r/\delta f$).

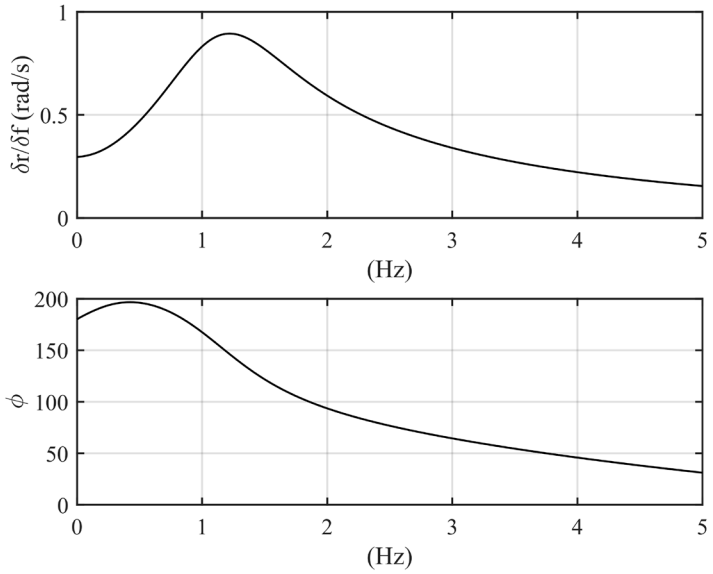

Figure 2. Amplitude and phase of the frequency response $\delta r/\delta f$ of the plant linearised for a longitudinal speed $V_0 = 100$ km/h and for $f_0 = 0.5$.

The thus obtained transfer function of the plant will be used in the next step to compute the open-loop performances of the system. The analysis is carried out considering the output that has to be tracked, δr, and the control input, δf.

2.4 Controller design

In Figure 3 a simplified schematic of the controller shows how the front-to-total anti-roll moment ratio is generated, starting from the measured/estimated variables of the vehicle. The desired anti-roll moment ratio f is given by two contributions: i) a feedforward contribution f_{FF} computed via the quasi-static model ([12] and [13]); ii) a feedback contribution f_{FB} is generated from a PI (i.e. proportional-integral) scheme. The PI controller gains vary with the vehicle speed v_x in a gain-scheduling fashion. The reference yaw rate and the feedforward contribution are modified based on the value of the rear axle side slip angle β_{RA} and lateral acceleration a_y by the two modifier blocks. This is done when β_{RA} and/or a_y exceed some threshold values set by design, in order to avoid unstable behaviour of the vehicle.

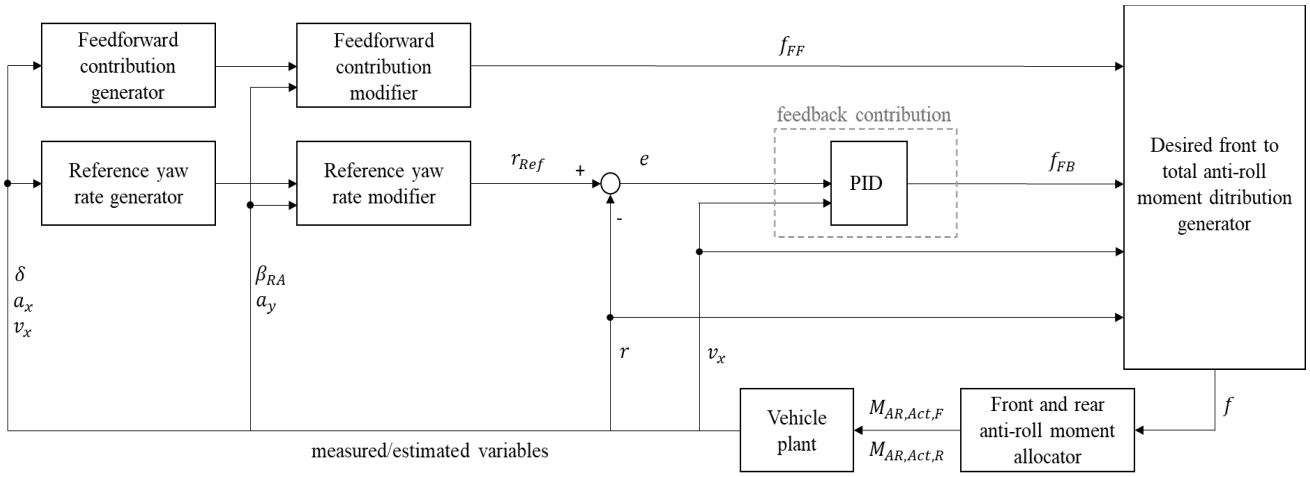

Figure 3. Simplified schematic of the controller

The output of the feedback controller is combined with the feedforward action weighting the two contributions depending on the steady-state value of the vehicle lateral acceleration (i.e. computed multiplying the actual values of vehicle speed and yaw rate). After the computation of the final front-to-total anti-roll moment ratio f the allocator block generates the front active anti-roll moment $M_{AR,Act,F}$ and the rear active anti-roll moment $M_{AR,Act,R}$, which are then sent as control action to the suspension actuators. The yaw rate error used as input of the feedback controller is given by:

$$e = r - r_{Ref} \tag{20}$$

where r_{ref} is computed through an optimisation routine using the quasi-static model in steady-state conditions and r is the measured yaw rate of the vehicle.

In order to consider the delay of the suspension actuators a first order transfer function multiplied for a pure time delay is used herein:

$$TF_{Actuator} = \frac{e^{-\tau_1 s}}{\tau_2 s + 1} \tag{21}$$

where τ_1 and τ_2 are the time constants such that $\tau_1 \neq \tau_2$. In this paper τ_1 is assumed to be 0.015 s and τ_2 is calculated starting from experimentally measured actuator cut off frequency of 6.6 Hz:

$$\tau_2 = \frac{1}{2\pi f} = 0.024 \ s \tag{22}$$

The plant of the systems used to design the PI controller is represented by the product:

$$G_{Plant} = \frac{e^{-\tau_1 s}}{\tau_2 s + 1} \left(\frac{\delta r}{\delta f} \right) \tag{23}$$

where $\delta r / \delta f$ is the relevant transfer function in Laplace domain that can be obtained from the state space of the model. The generic transfer function of the PI controller is the following:

$$G_{PI} = K_P + \frac{K_I}{s} \tag{24}$$

with K_P and K_I proportional and integral gains. Therefore, the open-loop transfer function of the system can be calculated as:

$$L(s \ = G_{Plant} G_{PI} = \left(\frac{e^{-\tau_1 s}}{\tau_2 s + 1} \right) \left(\frac{\delta r}{\delta f} \right) \left(K_P + \frac{K_I}{s} \ \right) \tag{25}$$

Whereas the closed-loop transfer function is:

$$T(s \ = \frac{L(s}{1 + L(s} \tag{26}$$

The PI gains are obtained using an optimisation procedure that will be fully explained in the remainder of this section. The optimisation problem considers as non-linear constraints the performance indicators (gain margin and phase margin) related to the $L(s$ transfer function response in the frequency domain. The mathematical definitions of the gain margin (GM) and phase margin (PM) are:

$$\begin{aligned} GM &= \frac{1}{|L(j\omega_{180} \ |} \\ PM &= \phi\big(L(j\omega_c \ \big) + 180^{\circ} \end{aligned} \tag{27}$$

where ω_{180} is the phase crossover frequency and ω_c is the gain crossover frequency when:

$$|L(j\omega_c\ |=1 \tag{28}$$

Suggested values of the gain margin and phase margin thresholds from the literature [14] for the stability of the system are assumed as follows:

$$\begin{aligned} GM &> 2 \\ PM &> 30^{\circ} \end{aligned} \tag{29}$$

The Matlab *fmincon* function is used for the optimisation process. The specific command finds the minimum of constrained non-linear multivariable functions. The cost function to be minimised is based on the rise time, the overshoot and settling time of a step response of the closed-loop transfer function. The rise time is the time it takes for the output to reach for the first time the 90 % of its final steady-state value; the overshoot is the value of the first peak of the response divided by its steady-state value; the settling time is the time needed by the response curve to settle within $\pm 5\%$ of the final value.

The cost function implemented in the optimisation loop results as follows:

$$CF = \ W_1\overline{t_r} + W_2\overline{OS} + W_3\overline{t_{set}} \tag{30}$$

where $\overline{t_r}$, $\overline{OS}$ and $\overline{t_{set}}$ are the values of actual rise time, overshoot and settling time scaled with some characteristic values.

W_1, W_2 and W_3 are the weight factors of the cost function which is:

$$CF = \ W_1\left(\frac{t_r}{t_{r,chr}}\right) + W_2\left(\frac{OS}{OS_{chr}}\right) + W_3\left(\frac{t_{set}}{t_{set,chr}}\right) \tag{31}$$

where $t_{r,chr}$, OS_{chr} and $t_{set,chr}$ are the characteristic values of the rise time, overshoot and settling time, respectively. For this study the following values are used:

$$\begin{aligned} t_{r,chr} &= 0.10 \text{ s} \\ OS_{chr} &= 20\ \% \\ t_{set,chr} &= 0.85 \text{ s} \end{aligned} \tag{32}$$

2.4.1 Optimisation procedure results: controller gains

The presented procedure is carried out for the three values of lateral acceleration (i.e. 3 m/s^2, 6 m/s^2 and 9 m/s^2) and three values of longitudinal speed (i.e. 60, 80, 100 km/h), thus obtaining nine different sets of gains for the controller. Table II report the values of controller gains, GM and PM, obtained as discussed.

TABLE II. GAIN SCHEDULING AND STABILITY INDICATORS

V [km/h]	60				80				100			
a_y [m/s^2]	$K_{P,1}$ [s/rad]	$K_{I,1}$ [1/rad]	GM_1 [-]	PM_1 [deg]	$K_{P,1}$ [s/rad]	$K_{I,1}$ [1/rad]	GM_1 [-]	PM_1 [deg]	$K_{P,1}$ [s/rad]	$K_{I,1}$ [1/rad]	GM_1 [-]	PM_1 [deg]
3	475,77	4871,9	2,35	50,21	244,9	2193,9	2,09	39,4	112,9	790,7	2,62	49,55
6	49,9	590,9	2	36,52	27,3	151,6	2,01	36,81	16,1	58,8	2	35,26
9	7,6	28,2	2,25	40,22	4,9	12,5	2,64	46,22	3,4	9,7	3,07	50,31

2.5 Simulation with validated vehicle model

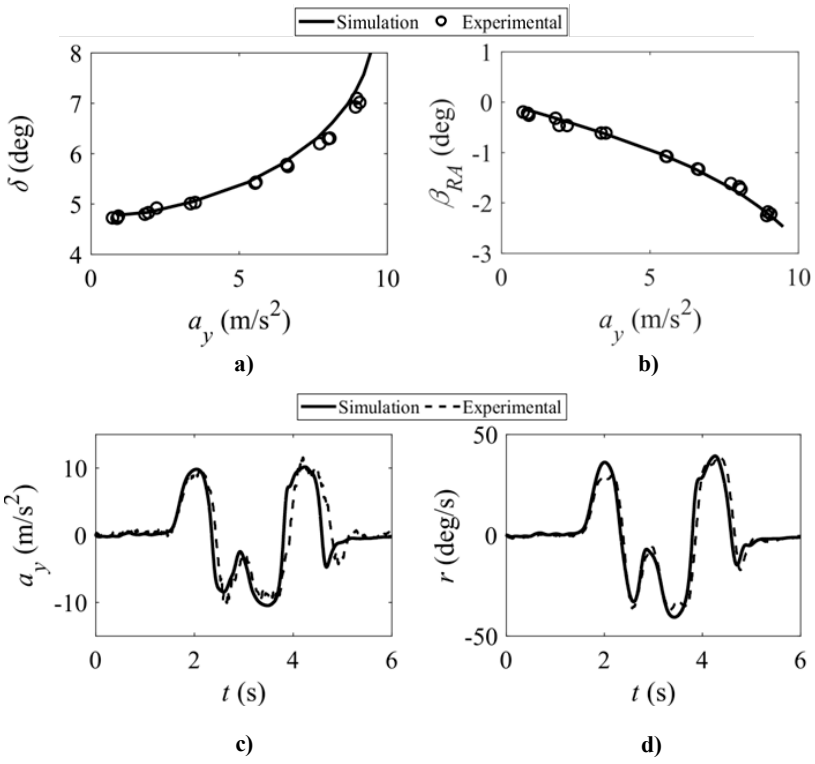

Figure 4. Nonlinear simulation model validation results in terms of: (a) understeer characteristics, (b) rear axle sideslip angle characteristics, (c) lateral acceleration as a function of time and (d) yaw rate as a function of time

The dynamic behaviour of an electric SUV equipped with active suspensions is simulated with an experimentally validated non-linear Matlab-Simulink model, which takes into account the same degrees of freedom of the quasi-static model in [12] and [13].

In Figure 4 the validation results for the model against experimental results employing the passive vehicle are reported during a skidpad test. Given the good match between simulations and experimental data, the model can be considered reliable for controller assessment.

2.5.1 Double step steer manoeuvre

Figure 5 reports the profiles of the main variables during the simulation of a double step steer from an initial speed of 100 km/h, with high tyre-road friction conditions.

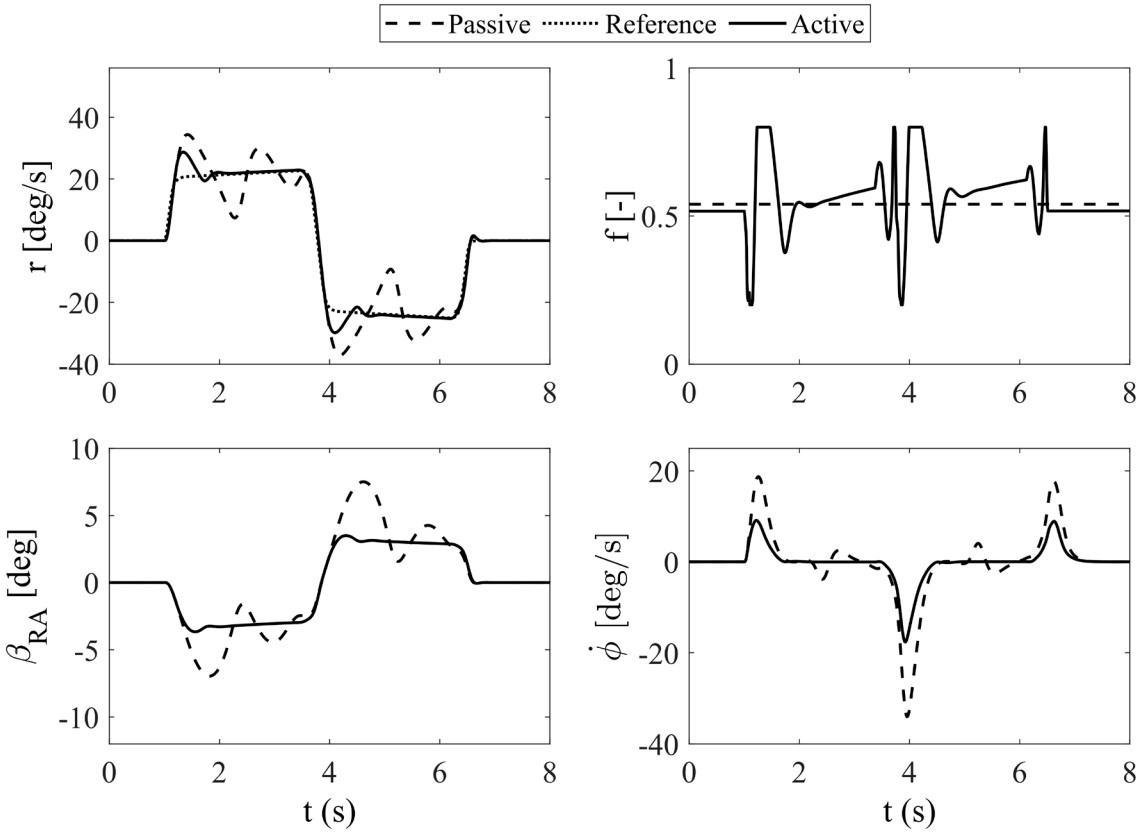

Figure 5. Double step steer simulation results for an initial speed of 100 km/h and μ=1 in terms of: yaw rate, front-to-total anti-roll moment distribution, rear axle side slip angle and roll rate

The simulated manoeuvre consists of a first steering wheel angle variation from 0 deg to 150 deg, a second step from 150 deg to -150 deg, and a final step that brings the steering wheel angle back to 0 deg. All steering angle variations are performed at 400 deg/s. Moreover, during the whole manoeuvre the total traction torque demand was set to zero. The results of the controlled configurations are reported together with those of the passive vehicle, i.e., the vehicle without active suspension functionality, nor stability control actuated through friction brakes.

The results show a significant improvement of the vehicle behaviour using the active suspensions. In particular, the active vehicle shows, for the vehicle yaw rate and sideslip angle, reduced overshoots and settling times compared to the passive vehicle. Tables III and IV report RMS (root mean square) and peak values of the yaw rate error and the rear axle sideslip angle β_{RA}, for each of the six controlled cases and for the passive vehicle.

TABLE III. RMS AND PEAK VALUES OF YAW RATE ERROR

Yaw rate error	Active Vehicle	Passive Vehicle
RMS (deg/s)	1.19	4.35
Peak value (deg/s)	7.19	15.59

TABLE IV. RMS AND PEAK VALUES OF REAR AXLE SIDE SLIP ANGLE

β_{RA}	Active Vehicle	Passive Vehicle
RMS (deg)	1.58	2.53
Peak value (deg)	3.28	7.51

The use of an active suspension system with anti-roll moment distribution control provide a significant improvement with respect to the passive vehicle.

3 Full 6-DoF vehicle model with suspension kinematics

As seen before, in the context of model-based design, the fidelity of the vehicle model to be used as plant of our system is of paramount importance. In the previous example the model that has been used is based on the bicycle model, that is a really simplified model which implies many approximations. With the bicycle model for example the vertical and pitch dynamics of the body and the suspension geometry are completely neglected, but if we are interested in implementing an ICC it may be necessary to consider all of these variables.

For these reasons a more complex vehicle model has to be developed in which we consider six degrees of freedom for the vehicle body, and, in order to properly model the exchange of forces between the tires and the body of the vehicle, also the suspension kinematic will be taken into account. This will result very important because with the suspension kinematic is possible to introduce into the model the Jacking forces, which in some cases have a big impact on the vertical dynamic of the body and on vertical tire loads.

In this chapter all the procedure needed to obtain the model will be described, but first some basic concepts about rotation matrices are introduced in order to better understand the following sections. This procedure has been developed following the one proposed in *The automotive chassis: volume 2: system design* (G. Genta and L. Morello, 2008).

3.1 Rotation matrices

In order to describe the motion of the system we define three reference systems:

1. Fixed reference frame $OXYZ$, where the plane XY is parallel to the ground and O lies on the latter.
2. The body reference frame Gxyz, which is fixed respect to the vehicle body (suspended mass), is centred in its centre of gravity, and its axis are parallel to the body principal axis of inertia.
3. The intermediate reference frame $Hx^*y^*z^*$, which is parallel to the ground and the origin H lies on the ground. The frame is rotated along the Z-axis until the x^*-axis is parallel to the projection of x on the ground. In this case the z^*-axis is equivalent to the Z-axis so the frame can be referred as Hx^*y^*Z .

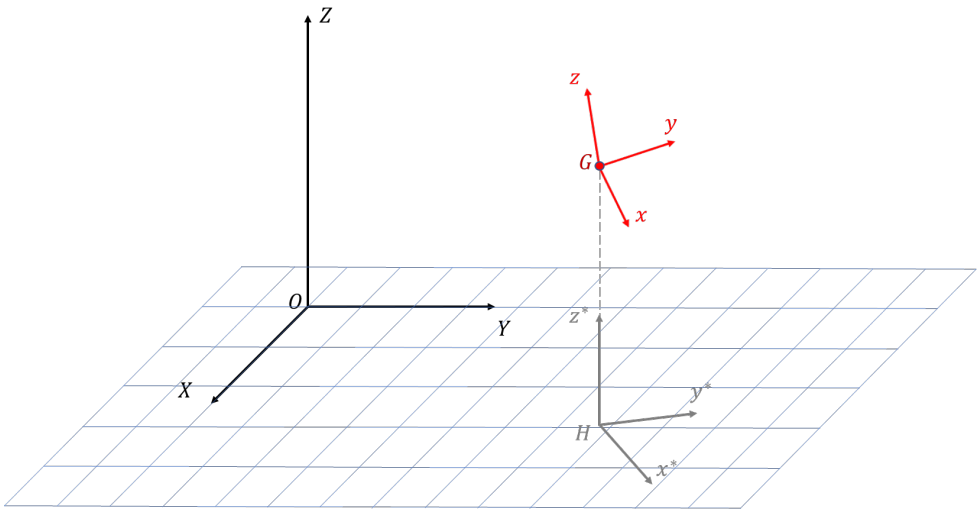

Figure 6: Reference frames

The position of the rigid body is thus defined if the position of G is known in the fixed reference frame, and ones the transformation matrix to pass from $OXYZ$ to Gxyz is defined.

The intermediate frame follows the vehicle translation along the ground plane and present the same rotation of the body reference frame along the Z-axis. It will result useful in order to properly define the longitudinal and lateral speed of each wheel, and thus obtain the side slip angles of the wheels.

3.1.1 Rotation matrices - Euler angle

In order to define the rotation of the body reference frame Gxyz and the intermediate frame Hx^*y^*Z respect to the fixed reference frame OXYZ it is possible to use 3x3 rotation matrices. The latter can be obtained by considering a sequence of three rotations about the axis of the frame, and in this case the order in which the rotations are performed influence the final rotation of the axis.

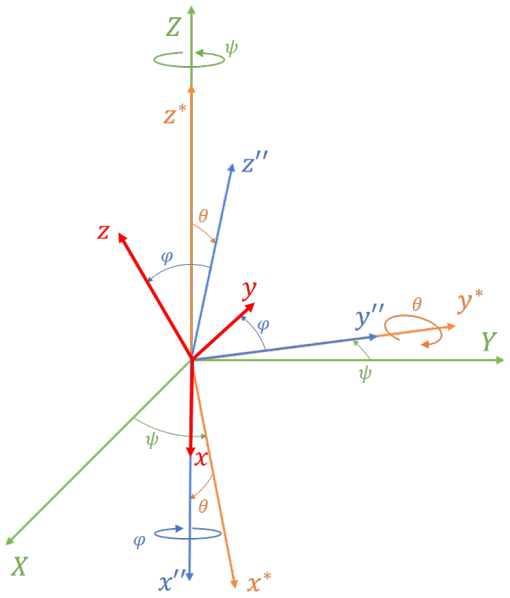

Figure 7: Tait - Bryan angles definition

The rotation of the Gxyz frame is thus defined by means of the Tait-Bryan angles, where the three rotation are performed in the order $Z \rightarrow Y \rightarrow X$ (Figure 7), while the intermediate frame Hx^*y^*Z is subject only to the rotation along the Z axis.

Each rotation is defined by a rotation matrix, which in this case are:

1. First rotation (Z-axis): The XYZ reference frame is rotated about the Z-axis of a ψ angle, thus defining the intermediate reference frame x^*y^*Z. The angle ψ is named yaw angle, and the matrix that defines the respective rotation is the following:

$$R_z = \begin{bmatrix} \cos(\psi & -sin(\psi & 0 \\ sin(\psi & \cos(\psi & 0 \\ 0 & 0 & 1 \end{bmatrix} \tag{33}$$

2. Second rotation (y^*-axis): The rotated reference frame x^*y^*Z is subject to a second rotation about the y^*-axis of a θ angle, which leads to the second rotated reference frame $x''y''z''$. The angle θ is named pitch angle, and the matrix that defines the respective is the following:

$$R_y = \begin{bmatrix} \cos(\theta & 0 & sin(\theta \\ 0 & 1 & 0 \\ -sin(\theta & 0 & \cos(\theta \end{bmatrix} \tag{34}$$

3. Third rotation (x''-axis): The second rotated reference frame $x''y''z''$ is subject to the final rotation about the x''-axis of a φ angle, which leads to the final reference frame xyz. The angle φ is named roll angle, and the matrix that defines the respective is the following:

$$R_x = \begin{bmatrix} 1 & 0 & 0 \\ 0 & \cos(\varphi & -sin(\varphi \\ 0 & sin(\varphi & \cos(\varphi \end{bmatrix} \tag{35}$$

The rotation matrix obtained by multiplying R_x, R_y and R_z is the transformation matrix which allows to write any vector in the body reference frame xyz to be written in the fixed reference frame XYZ:

$$R = R_z R_y R_x$$

$$R = \begin{bmatrix} c(\psi\ c(\theta & c(\psi\ s(\theta\ s(\varphi\ - s(\psi\ c(\varphi & c(\psi\ s(\theta\ c(\varphi\ + s(\psi\ s(\varphi \\ s(\psi\ c(\theta & s(\psi\ s(\theta\ s(\varphi\ + c(\psi\ c(\varphi & s(\psi\ s(\theta\ c(\varphi\ - c(\psi\ s(\varphi \\ -s(\theta & c(\theta\ s(\varphi & c(\theta\ c(\varphi \end{bmatrix} \tag{36}$$

Where cos and sin have been substituted with c and s, respectively, for the sake of clarity. The values of roll, pitch and yaw angle of the vehicle are not constant, indeed they vary with time thus the rotation matrix is not a constant matrix, but it's a time dependent matrix (when referring to the rotation matrix the dependence is implied, so instead of $R(t$ only R will be reported).

In this formulation the roll angle, φ, the pitch angle, θ, and the yaw angle can assume large values so the trigonometric functions containing the latter cannot be linearised with a first order Taylor expansion.

The rotation matrix R becomes:

$$R \approx \begin{bmatrix} \cos(\psi & -\sin(\psi & 0 \\ \sin(\psi & \cos(\psi & 0 \\ 0 & 0 & 1 \end{bmatrix} \bullet \begin{bmatrix} c(\theta & s(\theta\ s(\varphi & s(\theta\ c(\varphi \\ 0 & c(\varphi & -s(\varphi \\ -s(\theta & c(\theta\ s(\varphi & c(\theta\ c(\varphi \end{bmatrix} \tag{37}$$

$$R \approx R_z R_{yx}$$

The rotation matrix to pass from the body reference frame to the intermediate reference frame $R_{yx} = R_y R_x$ is:

$$R_y R_x = \begin{bmatrix} c(\theta & s(\theta\ s(\varphi & s(\theta\ c(\varphi \\ 0 & c(\varphi & -s(\varphi \\ -s(\theta & c(\theta\ s(\varphi & c(\theta\ c(\varphi \end{bmatrix} \tag{38}$$

Using the rotation matrix, it is possible to compute the coordinate in the fixed reference frame ($\{X, Y, Z\}^T$) of a point which coordinated are known in the body reference frame ($\{x, y, z\}^T$):

$$\begin{Bmatrix} X \\ Y \\ Z \end{Bmatrix} = R \begin{Bmatrix} x \\ y \\ z \end{Bmatrix} \tag{39}$$

If instead we write the transformation between the moving reference frame xyz and the intermediate reference frame $x^* y^* Z$, the only rotations involved are roll and pitch, thus the rotation matrix needed to pass from the first to the second frame is just R_{yx}. The use of the intermediate reference frame will be helpful in the next sections because the coordinates written in this frame do not depend on the yaw angle, thus the system can be linearised easily. If we want to pass from the intermediate frame to the fixed one, we need to apply the yaw rotation, thus the rotation matrix R_z:

$$\begin{Bmatrix} X \\ Y \\ Z \end{Bmatrix} = R_z R_{yx} \begin{Bmatrix} x \\ y \\ z \end{Bmatrix} = R_z \begin{Bmatrix} x^* \\ y^* \\ Z \end{Bmatrix} \tag{40}$$

In general, a rotation matrix is an orthogonal matrix ($R^{-1} = R^T$), thus:

$$R R^T = I \tag{41}$$

By deriving the equation above:

$$\dot{R}R^T + R\dot{R}^T = 0 \tag{42}$$

And by differentiating $\dot{R}R^T = S$, the following relations are obtained:

$$\begin{aligned} \dot{R} &= SR \\ S + S^T &= 0 \end{aligned} \tag{43}$$

S is a skew-symmetric matrix, so it contains only 3 independents elements and is defined as:

$$S(w \ = \begin{bmatrix} 0 & -w_z & w_y \\ w_z & 0 & -w_x \\ -w_y & w_x & 0 \end{bmatrix} \tag{44}$$

Where $\{w\} = [w_x \ w_y \ w_z]^T$ is a generic vector and for all $w, p \in R^3$ it holds:

$$S(w \ \cdot \{p\} = \{w\} \wedge \{p\} \tag{45}$$

3.1.2 Speed of a generic point P

The position respect to OXYZ of a generic point P of the rigid body, defined by the constant vector $\{p'\}$ in the body reference frame Gxyz, can be computed with the following relationship:

$$\{p\} = \{p_G\} + R \cdot \{p'\} \tag{46}$$

Where $\{p\} = \{X_P, Y_P, Z_P\}$ and $\{p_G\} = \{X_G, Y_G, Z_G\}$ define the position of P and G, respectively, in the OXYZ reference frame. The speed of P in the fixed reference frame is computed as:

$$\{\dot{p}\} = \{\dot{p}_G\} + \dot{R} \cdot \{p'\} + R \cdot \{\dot{p}'\} \tag{47}$$

Given that $\{p'\}$ is a constant vector and substituting equation Equation (43) it follows:

$$\{\dot{p}\} = \{\dot{p}_G\} + SR \cdot \{p'\} \tag{48}$$

Which, given Equation (45), is equal to:

$$\{\dot{p}\} = \{\dot{p}_G\} + \{W\} \wedge R \cdot \{p'\} \tag{49}$$

Where $\{W\} = \{\dot{\varphi}\ \dot{\theta}\ \dot{\psi}\}^T$ are the rotational speeds of the body reference frame respect to the non-rotated reference frame (in this case the angular ratio in the fixed reference frame and the intermediate one are equivalent). The angular speeds obtained by taking the first derivative of the Euler angles $\dot{\psi}$, $\dot{\theta}$ and $\dot{\varphi}$ are applied along the Z, y' and x'' axis, so to obtain the angular speeds in the body reference frame (rotations along x, y and z) a transformation matrix is needed:

$$\begin{Bmatrix} \Omega_x \\ \Omega_y \\ \Omega_z \end{Bmatrix} = \begin{Bmatrix} \dot{\varphi} \\ 0 \\ 0 \end{Bmatrix} + R_x^T \cdot \begin{Bmatrix} 0 \\ \dot{\theta} \\ 0 \end{Bmatrix} + R_{yx}^T \cdot \begin{Bmatrix} 0 \\ 0 \\ \dot{\psi} \end{Bmatrix} \tag{50}$$

In matrix form:

$$\begin{Bmatrix} \Omega_x \\ \Omega_y \\ \Omega_z \end{Bmatrix} = \begin{bmatrix} 1 & 0 & -\sin(\theta \\ 0 & \cos(\varphi & \sin(\varphi\ \cos(\theta \\ 0 & -\sin(\varphi & \cos(\varphi\ \cos(\theta \end{bmatrix} \cdot \begin{Bmatrix} \dot{\varphi} \\ \dot{\theta} \\ \dot{\psi} \end{Bmatrix} = E \cdot \begin{Bmatrix} \dot{\varphi} \\ \dot{\theta} \\ \dot{\psi} \end{Bmatrix} \tag{51}$$

And taking the inverse:

$$\begin{Bmatrix} \dot{\varphi} \\ \dot{\theta} \\ \dot{\psi} \end{Bmatrix} = \begin{bmatrix} 1 & \sin(\varphi\ \tan(\theta & \cos(\varphi\ \tan(\theta \\ 0 & \cos(\varphi & -\sin(\varphi \\ 0 & \sin(\varphi\ /\cos(\theta & \cos(\varphi\ /\cos(\theta \end{bmatrix} \cdot \begin{Bmatrix} \Omega_x \\ \Omega_y \\ \Omega_z \end{Bmatrix} = E^{-1} \cdot \begin{Bmatrix} \Omega_x \\ \Omega_y \\ \Omega_z \end{Bmatrix} \tag{52}$$

Which is not defined at $\theta = \pm\frac{\pi}{2}$, but in this case of study the pitch angle θ is by far within the limit values, so the matrix is well defined. By using these matrices is it possible to pass from the angular speed expressed in the body reference frame to the rate of change of the Euler angles, and vice versa.

3.2 Model description

In first approximation, the suspension can be modelled as a rigid link between the centre of the tire contact patch, indicated in Figure 8 as T_i, and the instantaneous centre of rotation of the suspension respect to the vehicle body, indicated as J_i.

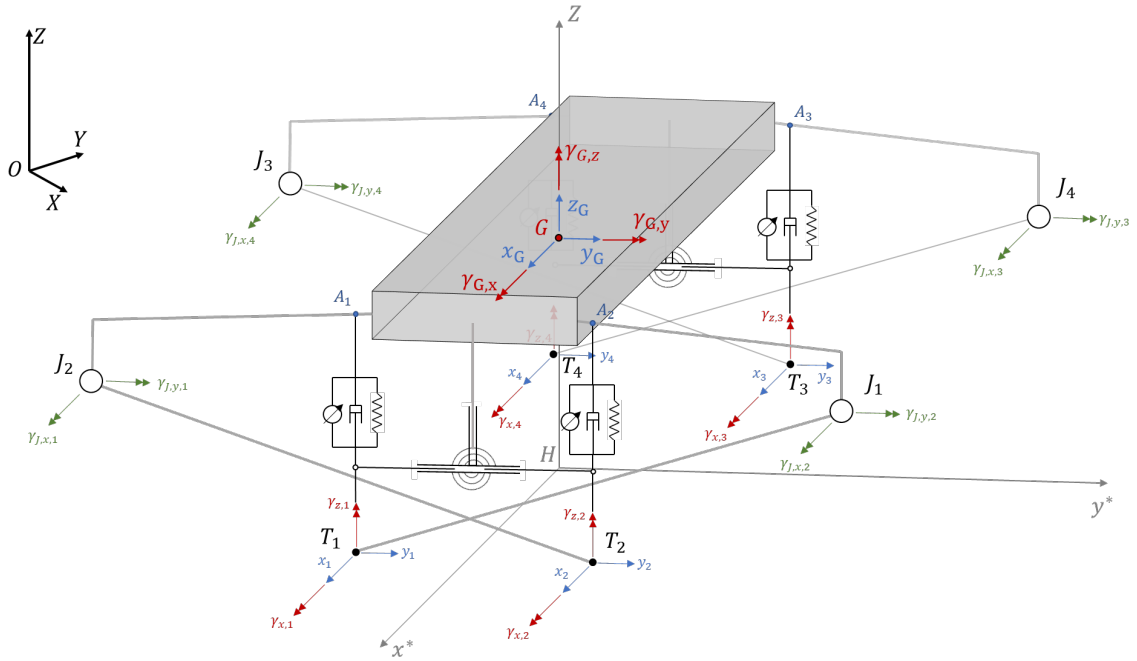

Figure 8: Schematic of the 6 DoF model

Each suspension is thus composed by a rigid link and a subsystem containing spring, damper ad actuator, which are assumed to exchange forces with the tire and the body only in vertical direction between the points T_i and A_i. The effect of anti-roll bars is taken into account by beans of two torsional springs between the body and the suspension, in order to generate vertical load transfer at the wheels when the vehicle is subject to roll. In general, the position of each point J_i depends on suspension geometry, and it

varies according to the body movements. Its trajectory can be analytically described only by knowing the kinematic of the specific suspensions, so is not possible to have a general-purpose model, valid for different kind of suspensions, if the position of the points J_i is given by kinematic equations.For this reason, the position of the points J_i has been assumed to be constant, respect to the body, around a linearisation point. By doing this approximation the four J_i are rigidly linked to the body during movement around the linearisation point, and the only data needed to properly describe the suspensions are the positions of these points, respect to the body, only in the linearisation point chosen to obtain the linearised model.

3.2.1 Computation of the Degrees of Freedom of the system

The model in Figure 8 is composed by 5 rigid bodies: 4 massless rigid links to model the four suspensions, and 1 rigid body that represent the suspended mass of the vehicle. Each one of the five rigid bodies have 6 Degrees of Freedom in the space (3 translations + 3 rotations), so the system presents a total of 30 DoF. The number of degrees of freedom is reduced by introduction of the following kinematic constraints:

- The four point T_1, T_2, T_3 and T_4 represent the contact point between the tires and the ground; These points are free to move in the plane XY and the allowed rotations are $\gamma_{x,i}$ and $\gamma_{z,i}$, so each one of these points maintain four degrees of freedom, while the other 2 are locked by the constraints (displacement along z and rotation along y).
- The four point J_1, J_2, J_3 and J_4 represent the points of instantaneous rotation for the four suspensions respect to the vehicle body; In these points, the only movements allowed between the links and the suspended mass are the two rotation $\gamma_{J,x,i}$ (to allow roll motion) and $\gamma_{J,y,i}$ (to allow pitch motion). The four joints remove 4 degrees of freedom, allowing only the two rotations described above.

At this point the number of degrees of freedom of the constrained system can be computed as:

$$\begin{gathered} F = B \cdot l - 4 \cdot n_J - 2 \cdot n_T \\ B = \text{number of bodies} \\ l = \text{number of DoF for each body (6 for a system in 3 dimensions)} \\ n_J = \text{number of joints of type J} \end{gathered} \tag{53}$$

$$n_T = \text{number of joints of type T}$$

Given that for the system showed above we have:

$$\begin{aligned} B &= 5 \\ l &= 6 \\ n_J &= 4 \\ n_T &= 4 \end{aligned} \tag{54}$$

The constrained system has $F = 6$, thus its motion is completely described by means of six generalised coordinates. The purpose of this model is that of describing the suspended mass dynamic, and for these reasons the 3 translations and the 3 rotations of the body centre of gravity have been chosen as generalised coordinates to describe the motion of the system. The systems which represent the anti-roll bars in Figure 8 have not been taken into account for the computation of the degrees of freedom because all the links that compose these system are completely constrained, so they don't add or remove any degree of freedom to the system.

3.3 Lagrange equations in terms of quasi-static coordinates

In this section the analytical method presented to obtain the equation of motion has been taken from the book *The automotive chassis: volume 2: system design* (G. Genta and L. Morello, 2008).

The equations of motion of the vehicle can be written by using the Lagrangian approach, writing the kinetic energy, T, and the potential energy, V, of the system using an arbitrary set of n generalised coordinates, thus obtaining the Lagrangian of the system:

$$L^*(\dot{q}_i, q_i, t \ = T^*(\dot{q}_i, q_i, t \ - V(q_i, t \qquad i = 1, \dots, n \tag{55}$$

Where q_i is the i-th generalised coordinate and $\dot{q}_i$ is the i-th generalised velocity, computed as the first derivative of the respective generalised coordinate.

Thus, the equations of motion are obtained by means of the following formulation:

$$\frac{d}{dt}\frac{\partial L^*}{\partial \dot{q}_i} - \frac{\partial L^*}{\partial q_i} + \frac{\partial D^*}{\partial \dot{q}_i} = Q_i \qquad i = 1, \dots, n \tag{56}$$

Where D^* is the Rayleigh dissipation function and Q_i are the generalised forces.

When dealing with Euler equation for the motion of a rigid body, it is usual to use a linear combination of the first derivatives of the generalised coordinates in order to define the generalised velocities:

$$\{w\} = A^T \cdot \{\dot{q}\} \tag{57}$$

Where A^T is a transformation matrix whose elements in general are function of the generalised coordinates. By computing the inverse of A^T is it possible to write the inverse transformation:

$$\{\dot{q}\} = B \cdot \{w\} \tag{58}$$

Where $B = A^{-T}$, and unless A is a rotation matrix, in general $B \neq A$.

The Lagrangian of the system is therefore written in terms of the "quasi-coordinates" $\{w_i\}$:

$$L(w_i, q_i, t \ = T(w_i, q_i, t \ - V(q_i, t \qquad i = 1, \dots, n \tag{59}$$

The derivatives in (56) are thus rewritten in order to obtain the equations of motion in terms of quasi-coordinates:

$$\frac{\partial T^*}{\partial \dot{x}_k} = \sum_{i=1}^{n} \frac{\partial T}{\partial w_i}\frac{\partial w_i}{\partial \dot{x}_k} \qquad k = 1, \dots, n \tag{60}$$

Which in matrix form becomes:

$$\left\{\frac{\partial T^*}{\partial \dot{x}}\right\} = A \left\{\frac{\partial T}{\partial w}\right\} \tag{61}$$

And by differentiating it respect to the time, the first term of Equation (56) is obtained:

$$\frac{\partial}{\partial t}\left(\left\{\frac{\partial T^*}{\partial \dot{x}}\right\}\right) = A\frac{\partial}{\partial t}\left(\left\{\frac{\partial T}{\partial w}\right\}\right) + \dot{A}\left\{\frac{\partial T}{\partial w}\right\} \tag{62}$$

The component $\dot{a}_{jk}$ of the matrix $\dot{A}$ can be computed as:

$$\dot{a}_{jk} = \left[w^T B^T \left\{ \frac{\partial a_{jk}}{\partial x} \right\} \right] \tag{63}$$

where the term a_{jk} is the corresponding component of the matrix A.

The second term of Equation (56) is obtained by means of the following equation:

$$\frac{\partial T^*}{\partial x_k} = \frac{\partial T}{\partial x_k} + \sum_{i=1}^{n} \frac{\partial T}{\partial w_i} \frac{\partial w_i}{\partial x_k} \qquad k = 1, \dots, n \tag{64}$$

Which can be written in matrix form as:

$$\left\{ \frac{\partial T^*}{\partial x} \right\} = \left\{ \frac{\partial T}{\partial x} \right\} + \left[w^T B^T \frac{\partial A}{\partial x} \right] \left\{ \frac{\partial T}{\partial w} \right\} \tag{65}$$

The potential energy, V, does not depend on the generalised velocities, so it is not influenced by the definitions of the latter.

Instead, the derivatives of the dissipation function are computed as:

$$\left\{ \frac{\partial D^*}{\partial \dot{x}} \right\} = A \left\{ \frac{\partial D}{\partial w} \right\} \tag{66}$$

The equation of motion for the system are thus written in terms of quasi-coordinates by substituting (62),(65) and (66) in (56):

$$\begin{aligned} \left\{ A \frac{\partial}{\partial t} \left(\left\{ \frac{\partial T}{\partial w} \right\} \right) + \left[w^T B^T \left\{ \frac{\partial a_{jk}}{\partial x} \right\} \right] \left\{ \frac{\partial T}{\partial w} \right\} \right\} - \left\{ \left\{ \frac{\partial T}{\partial x} \right\} + \left[w^T B^T \frac{\partial A}{\partial x} \right] \left\{ \frac{\partial T}{\partial w} \right\} \right\} + \left\{ \frac{\partial V}{\partial x} \right\} \\ + A \left\{ \frac{\partial D}{\partial w} \right\} = \{Q\} \end{aligned} \tag{67}$$

Which, by collecting the term $\{\frac{\partial T}{\partial w}\}$, becomes:

$$A \frac{\partial}{\partial t} \left(\left\{ \frac{\partial T}{\partial w} \right\} \right) + \Gamma \left\{ \frac{\partial T}{\partial w} \right\} - \left\{ \frac{\partial T}{\partial x} \right\} + \left\{ \frac{\partial V}{\partial x} \right\} + A \left\{ \frac{\partial D}{\partial w} \right\} = \{Q\} \tag{68}$$

where:

$$\Gamma = \left[w^T B^T \left\{ \frac{\partial a_{jk}}{\partial x} \right\} \right] - \left[w^T B^T \frac{\partial A}{\partial x} \right] \tag{69}$$

and $\{Q\}$ is the vector of generalised forces written in terms of the generalised coordinates $\{q\}$.

The final system is obtained by premultiplying by $B^T = A^{-1}$ and by adding the six kinematic equation to pass from the quasi-coordinates $\{w\}$ to the real generalised velocities $\{\dot{q}\}$:

$$\begin{cases} \dfrac{\partial}{\partial t}\left(\left\{ \dfrac{\partial T}{\partial w} \right\} \right) + B^T \Gamma \left\{ \dfrac{\partial T}{\partial w} \right\} - B^T \left\{ \dfrac{\partial T}{\partial x} \right\} + B^T \left\{ \dfrac{\partial V}{\partial x} \right\} + \left\{ \dfrac{\partial D}{\partial w} \right\} = B^T \{Q^*\} \\ \{\dot{q}\} = B\{w\} \end{cases} \tag{70}$$

3.3.1 Application to the vehicle model

In the field of vehicle dynamics, in order to obtain the equation of motion it is very convenient to use the generalised coordinates defined respect to the body reference frame, which being a principal frame of inertia leads to a simplified equation for the kinetic energy.

However, the body reference frame is a non-inertial reference frame that rotates constantly so is not possible to compute the displacement of the system in this frame by integrating the velocities in the same frame. To solve this problem, it is common to define the displacement and the velocities separately, thus maintaining the simplified equation for the kinetic energy and therefore simplified equation of motion. For this purpose, the generalised coordinates for the displacement are defined respect to the intermediate reference frame, while the generalised velocities are defined respect to the body reference frame.

The choice to use the intermediate frame, instead of the inertial reference, leads to a simplified formulation for the lateral and longitudinal displacements because the yaw rotation is not considered during the computation of the latter. However, by using this procedure the vertical displacement is not influenced (is the same in both the fixed and intermediate reference frame), but in the computation of the lateral virtual displacement also the contribution due to the yaw rotation has to be taken into account. In order to do this, the generalised velocities (expressed in the body frame) have to be expressed as a linear combination of the velocities in the intermediate frame, thus the transformation matrix to pass from one frame to the other has to be known.

In such a case, the vector of the generalised coordinates (in the intermediate reference frame) is:

$$\{q\} = \{x^*, y^*, Z, \varphi, \theta, \psi\}^T \tag{71}$$

While the vector of the generalised velocities, respect to the body reference frame, is:

$$\{w\} = \{v_x, v_y, v_z, \Omega_x, \Omega_y, \Omega_z\}^T \tag{72}$$

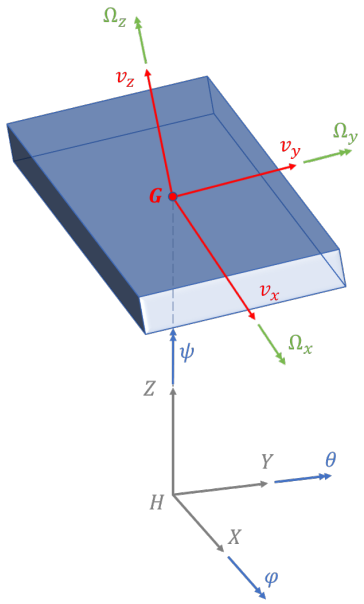

Figure 9: generalised coordinates and velocities

Where v_x, v_y and v_z are the velocities at the origin of the moving reference frame, thus of the vehicle centre of gravity.

This way the velocities vector can't be computed as first derivative of the generalised coordinates vector, but it is linked to the latter by means of the 6 kinematic equation from (39) and (51):

$$\begin{Bmatrix} v_x \\ v_y \\ v_z \end{Bmatrix} = R_{yx}^T \cdot \begin{Bmatrix} \dot{X} \\ \dot{Y} \\ \dot{Z} \end{Bmatrix} \tag{73}$$

$$\begin{Bmatrix} \Omega_x \\ \Omega_y \\ \Omega_z \end{Bmatrix} = E \cdot \begin{Bmatrix} \dot{\varphi} \\ \dot{\theta} \\ \dot{\psi} \end{Bmatrix}$$

And in matrix form:

$$\{w\} = A^T \cdot \{\dot{q}\} \tag{74}$$

Where:

$$A^T = \begin{bmatrix} R_{yx}^T & 0 \\ 0 & E \end{bmatrix} \tag{75}$$

Thus, writing the inverse transformation we get:

$$\{\dot{q}\} = B \cdot \{w\} \tag{76}$$

Where $B = A^{-T}$, and given that E is not a rotation matrix $A^{-1} \neq A^T$, thus $B \neq A$.

By using this set of generalised coordinates, given that the body reference frame is a principal frame of inertia, the kinetic energy of the system is:

$$T = \frac{1}{2} m(v_x^2 + v_y^2 + v_z^2) + \frac{1}{2}(I_x \Omega_x^2 + I_y \Omega_y^2 + I_z \Omega_z^2) \tag{77}$$

where m is the mass of the vehicle body and I_x, I_y and I_z are the moment of inertia of the vehicle along the three principal axis of inertia x, y and z, respectively.

The equation of motion of the system are thus obtained by means of the equation system in (70), and the matrix $B^T\Gamma$ in this case becomes:

$$B^T\Gamma = \begin{bmatrix} \widetilde{\Omega} & 0 \\ \tilde{V} & \widetilde{\Omega} \end{bmatrix} \tag{78}$$

$\widetilde{\Omega}$ and $\tilde{V}$ are skew-symmetric matrices which, according to [15], contain the components of the quasi-velocities:

$$\widetilde{\Omega} = \begin{bmatrix} 0 & -\Omega_z & \Omega_y \\ \Omega_z & 0 & -\Omega_x \\ -\Omega_y & \Omega_x & 0 \end{bmatrix} \qquad \widetilde{V} = \begin{bmatrix} 0 & -v_z & v_y \\ v_z & 0 & -v_x \\ -v_y & v_x & 0 \end{bmatrix} \tag{79}$$

At this point the equation of motion of the system can be written by means of (70).

3.3.2 Potential energy and dissipation function

The potential energy of the system is due to the gravity force acting on it and the energy stored in the springs reported in Figure 10. The system presents four linear springs, one for each suspension, and two torsional springs to model the effect of passive anti-roll bars.

The dissipation function, instead, is linked to the elements in which the dissipation of energy occurs as a result of viscous forces, thus it is linked with the four dampers present in the system.

Assuming that each of the four the subsystems composed by spring, damper and actuator remains vertical respect to the ground, in order to write the potential energy and the dissipation function of the system, it is sufficient to write the vertical displacement of the four point A_i in which the i-th subsystem transmit the forces to the vehicle body.

By knowing the position of A_i with respect to the centre of gravity of the vehicle it possible to write the vertical displacement and velocity of the respective point as a function of the generalised coordinates by means of (46) and (48), which provide the following relations:

$$\begin{aligned} \begin{Bmatrix} x^*_{A_i} \\ y^*_{A_i} \\ Z_{A_i} \end{Bmatrix} &= \begin{Bmatrix} x^*_G \\ y^*_G \\ Z_G \end{Bmatrix} + R_{yx} \cdot \{A'_i\} \\ \begin{Bmatrix} \dot{x}^*_{A_i} \\ \dot{y}^*_{A_i} \\ \dot{Z}_{A_i} \end{Bmatrix} &= \begin{Bmatrix} \dot{x}^*_G \\ \dot{y}^*_G \\ \dot{Z}_G \end{Bmatrix} + SR_{yx} \cdot \{A'_i\} \end{aligned} \tag{80}$$

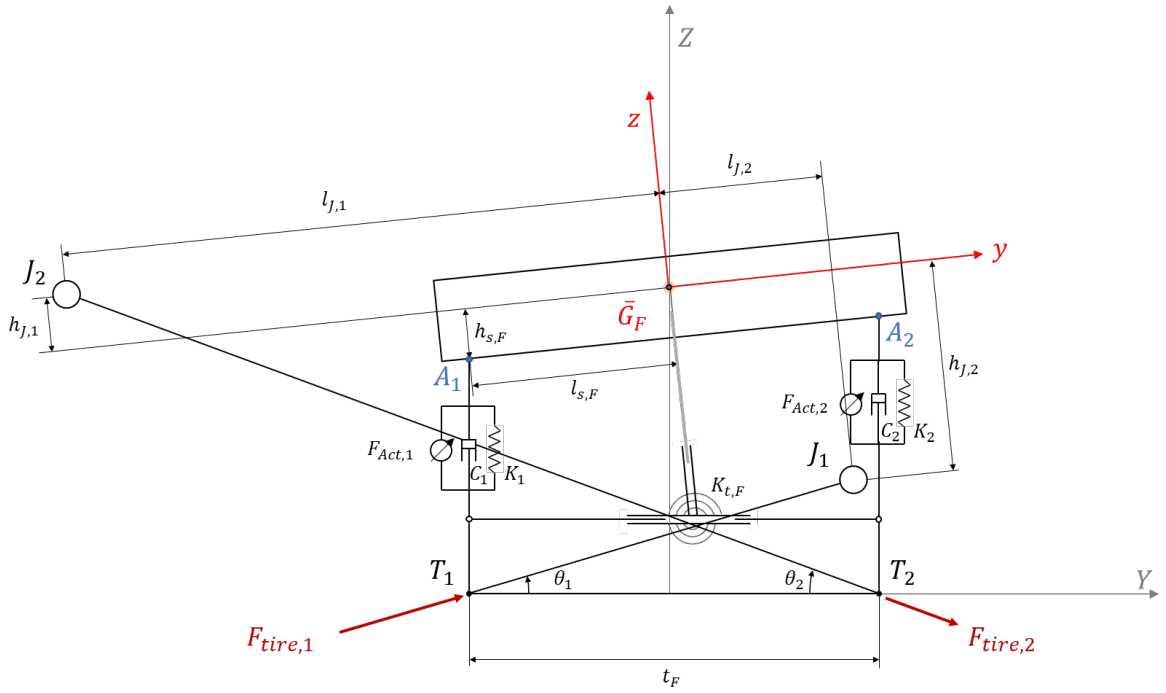

Figure 10: Front axle schematic during cornering

where the matrix S contains the variation ratios of the Euler angle:

$$S=\begin{bmatrix} 0 & -\dot{\psi} & \dot{\theta} \\ \dot{\psi} & 0 & -\dot{\varphi} \\ -\dot{\theta} & \dot{\varphi} & 0 \end{bmatrix} \tag{81}$$

and positions of the four points A_i respect to the CoG are:

$$A_1' = \begin{Bmatrix} a \\ -l_{s,F} \\ h_{s,F} \end{Bmatrix} \quad A_2' = \begin{Bmatrix} a \\ l_{s,F} \\ h_{s,F} \end{Bmatrix} \quad A_3' = \begin{Bmatrix} -b \\ l_{s,R} \\ h_{s,R} \end{Bmatrix} \quad A_4' = \begin{Bmatrix} -b \\ -l_{s,R} \\ h_{s,R} \end{Bmatrix} \tag{82}$$

in which a and b are, respectively, the front and rear semi-wheelbase.

By using these relations it is possible to write the potential energy, V, and the dissipation function, D, of the system:

$$V = \frac{1}{2}\sum_{i=1}^{4} K_i\left(Z_{A_i} - Z_{static,A_i}\right)^2 + \frac{1}{2}(K_{t,F} + K_{t,R})\varphi^2 + mgZ_G \tag{83}$$

$$D = \frac{1}{2}\sum_{i=1}^{4} C_i (\dot{Z}_{A_i})^2$$

where: K_i is the stiffness of the i-th spring, $K_{t,F}$ and $K_{t,R}$ are the front and rear anti-roll bars stiffness, and C_i is the damping coefficient of the i-th damper, and Z_{static,A_i} is the static value of Z_{A_i}.

As discussed before, instead of using the velocities in the fixed reference frame, it is convenient to use the quasi-coordinates respect to the moving reference frame.

The equation for the potential energy does not depend on the velocities of the system in the fixed reference frame, however the dissipation function depends on the latter so it needs to be rewritten in terms of quasi-velocities in the moving reference frame. In order to do that it is possible to pass from one system to the other by using (76), thus obtaining $\dot{Z}_{A_i}$ as a function of the quasi-velocities:

$$\dot{Z}_{A_i} = f(\dot{q} \ = g(w \tag{84}$$

And by replacing the equation above in (83) the dissipation function becomes a function of the quasi-velocities w.

3.3.3 Generalised forces

The generalised force vector can be obtained starting from the virtual work, δW, of the applied forces:

$$\delta W = \sum_{j=1}^{m} F_j \cdot \delta r_j \tag{85}$$

where δr_j is the virtual displacement of the point in which the j-th of the m force is applied.

Given that the position of a generic point can be written as a function of the generalised coordinates as $r_j = r_j(q_1, ..., q_n, t$, the virtual displacement can be written as:

$$\delta r_j = r_j(q_1, ..., q_n, t \ = \frac{\partial r_j}{\partial q_1}\delta q_1 + \cdots + \frac{\partial r_j}{\partial q_n}\delta q_n = \sum_{i=1}^{n} \frac{\partial r_j}{\partial q_i}\delta q_i \tag{86}$$

Thus, the virtual work becomes:

$$\delta W = \sum_{j=1}^{m} F_j \cdot \sum_{i=1}^{n} \frac{\partial r_j}{\partial q_i} \delta q_i = \sum_{i=1}^{n} \left(\sum_{j=1}^{m} F_j \frac{\partial r_j}{\partial q_i} \right) \delta q_i = \sum_{i=1}^{n} Q_i \delta q_i \tag{87}$$

The generalised Q_i represent the equivalent forces acting on the virtual displacements of the generalised coordinate q_i, and they are computed as:

$$Q_i = \sum_{j=1}^{m} F_j \frac{\partial r_j}{\partial q_i} \tag{88}$$

where m is the number of external forces acting on the system, and with this definition it can be proved that (70) is valid. In order to write the generalised forces, the virtual displacement have to be defined for each of the force applied to the system. The external forces in this case are: the four reaction forces of the tires and the force generated by the actuators; the latter, $F_{Act,i}$, act only in vertical direction in the A_i points, so the only virtual displacement needed is provided by the equation (80), and the virtual work related to the actuators is given by:

$$\delta W_{F_{Act}} = \sum_{i=1}^{4} F_{Act,i} \cdot \delta Z_{A_i} \tag{89}$$

The tires transmit their forces with the bodies in the four J_i points through the suspensions links, which can transmit only tensile or compression forces. Because of this, the forces acting on the J_i points have both lateral and a vertical component, thus requiring the computation of the vertical al lateral virtual displacement for these points. Under the assumption that the position vectors of the four joints are constant respect to the body reference frame during small oscillation around the linearisation point, according to Figure 10, they are defined as it follows:

$$J_1' = \begin{Bmatrix} a \\ l_{J,1} \\ h_{J,1} \end{Bmatrix} \quad J_2' = \begin{Bmatrix} a \\ -l_{J,2} \\ h_{J,2} \end{Bmatrix} \quad J_3' = \begin{Bmatrix} -b \\ -l_{J,3} \\ h_{J,3} \end{Bmatrix} \quad J_4' = \begin{Bmatrix} -b \\ l_{J,4} \\ h_{J,4} \end{Bmatrix} \tag{90}$$

Therefore, the virtual displacements are calculated by means of (46), similarly to what has been done for the A_i points. The lateral tire forces act along the direction of the y^* axis of the intermediate reference frame, while the vertical components transmitted to the body act along the Z axis. As said before in order to properly define the lateral virtual displacement also the contribution given by the yaw rotation has to be taken into account. To do that it is possible to use the rotation matrix R_z but, due to the fact that it will be used to compute infinitesimal displacement, in this case it is possible to use the small angle assumption also for the yaw angle, thus obtaining:

$$\delta R_z = \begin{bmatrix} 1 & -\delta\psi & 0 \\ \delta\psi & 1 & 0 \\ 0 & 0 & 1 \end{bmatrix} \tag{91}$$

The virtual displacement related to the J_i points are then computed by means of the following relation:

$$\begin{Bmatrix} \delta x^*_{J_i} \\ \delta y^*_{J_i} \\ \delta Z_{J_i} \end{Bmatrix} = \begin{Bmatrix} x^*_G \\ y^*_G \\ Z_G \end{Bmatrix} + \delta R_z R_{yx} \{J'_i\} \tag{92}$$

Thus the virtual work exerted by the lateral forces of the tires is:

$$\delta W_{F_y} = \sum_{i=1}^{4} F_{y,i} \cdot \delta y^*_{J_i} \tag{93}$$

While the virtual work of the vertical component of tire forces is:

$$\delta W_{F_J} = \sum_{i=1}^{4} F_{J,i} \cdot \delta Z_{J_i} \tag{94}$$

Once the virtual displacements have been obtained, for each one of the F_j forces, the generalised forces Q_i are computed by using (88).

3.4 Tire forces

In this section, the equations used to compute the forces exerted by the tires are reported. In our case, the forces generated by the contact between the tires and the ground are the lateral forces and the vertical forces only because we are not taking into account the longitudinal dynamic of the vehicle.
Moreover with this model it is possible to introduce the effect of the Jacking forces, which will be discussed in detail later.

3.4.1 Lateral forces

The force exerted by the tire is computed by means of the Pacejka formula in [8].
It's general form, that holds for given values of vertical load and camber angle, reads:

$$y = D\sin[C\tan^{-1}\{(1 - E\ \ Bx - E\tan^{-1}(Bx\ \}] \tag{95}$$

with

$$\begin{aligned} Y(X\ \ &= y(x\ \ + S_V \\ x &= X + S_H \end{aligned} \tag{96}$$

where Y is the output variable and is defined as the longitudinal force $F_x = y(k\ \ $ or the lateral force $F_y = y(\alpha\ \ $ or the aligning torque M_z. X is defined as the input variable and as input the longitudinal slip κ and side slip angle α can be used. The remaining variables of the Magic Formula describe the following coefficients:

- B stiffness factor
- C shape factor
- D peak value
- E curvature factor
- S_H horizontal shift
- S_V vertical shift

The Magic Formula y(x) typically produces a curve that passes through the origin x = y = 0, reaches a maximum and subsequently tends to a horizontal asymptote. To allow the curve to have an offset with respect to the origin, two shifts S_H and S_V have been introduced. A new set of coordinates Y(X) arises as shown in Figure 11.

The formula Equation (95) is capable of producing characteristics that closely match measured curves for the lateral force F_y (and if desired also for the aligning torque M_z) as a function of the slip angle α and for the longitudinal force F_x as a function of the longitudinal slip k. Both characteristics consider the effect of the vertical load F_z and a camber angle γ included in the parameters.

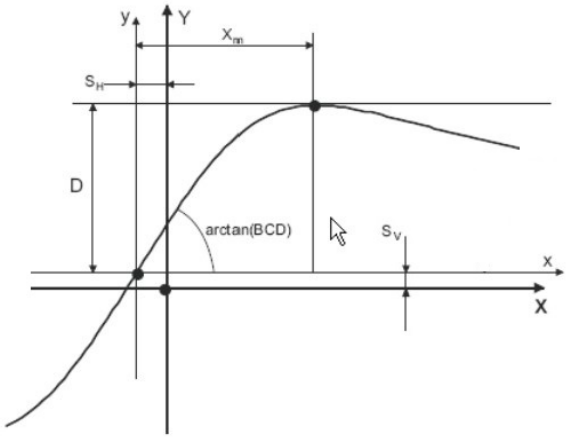

Figure 11. Curve produced by the original sine version of the Magic Formula

Coefficient D represents the peak value (for C ≥ 1) and the product BCD corresponds to the slope at the origin (x = y = 0). The shape factor C controls the limits of the range of the sine function appearing in (68) and thereby determines the shape of the resulting curve. The factor B is left to determine the slope at the origin and is called the stiffness factor. The factor E is introduced to control the curvature at the peak and at the same time the horizontal position of the peak x_m. The offsets S_H and S_V appear to occur when ply-steer (describes the lateral force a tire generates due to asymmetries in its carcass as is rolls forward with zero slip angle and may be called pseudo side slip)and conicity effects and possibly the rolling resistance cause the longitudinal and lateral curves not to pass to the origin. Wheel camber may give rise to a considerable offset of the F_y vs α curves.

The aligning torque M_z can now be obtained by multiplying the side force F_y with the pneumatic trail t (it is the distance that the resultant force of side-slip occurs behind the geometric centre of the contact patch)and adding the usually small (except with camber) residual torque M_{zr}.

$$M_z = -t * F_y + M_{zr} \tag{97}$$

The pneumatic trail decreases with increasing side slip and is described as:

$$t(\alpha_t \ = D_t \cos[C_t \tan^{-1}\{B_t\alpha_t - E_t(B_t\alpha_t - \tan^{-1}(B_t\alpha_t \ \}] \tag{98}$$

where

$$\alpha_t = \tan\alpha + S_{Ht} \tag{99}$$

The residual torque shows a similar decrease:

$$M_{zr}(\alpha_r \ = D_r \cos[\tan^{-1}(B_r\alpha_r \ ] \tag{100}$$

with

$$\alpha_r = \tan\alpha + S_{Hf} \tag{101}$$

Both the aligning and residual torque are modelled using the Magic Formula, but instead of the sine function, the cosine function is applied to produce a hill-shaped curve.

The residual torque is assumed to attain its maximum D_r at the slip angle where the side force becomes equal to zero. This is accomplished through the horizontal shift S_{Hf}. The peak of the pneumatic trail occurs at $\tan\alpha = -S_{Ht}$. The advantage with respect to the earlier versions, where formula (68) is used for the aligning torque as well, is that we have now directly assessed the function for the pneumatic trail which is needed to handle the combined slip situation.

The measured tire characteristics may be not entirely symmetric, for example $F_y(\alpha, \gamma \ \neq -F_y(-\alpha, -\gamma$. This can be caused the tire characteristics conicity and ply steer or inaccuracies in the measurements. In this case, it is preferable to eliminate these offsets and asymmetry and have a completely symmetric tire in the simulation environment. In that case the following parameters should be set zero and kept zero in

the identification process: rHx1, qsx1, pEy3, pHy1, pHy2, pVy1, pVy2, rBy3, rVy1, rVy2, qBz4, qDz6, qDz7, qEz4, qHz1, qHz2, ssz1, and qDz3.

The effect of having a tire with a different nominal load may be roughly approximated by using the scaling factor $\lambda_{F_{z0}}$:

$$F'_{z0} = \lambda_{Fzo} F_{z0} \tag{102}$$

Further, we introduce the normalized change in vertical load

$$df_z = \frac{F_z - F'_{z0}}{F'_{z0}} \tag{103}$$

In the Simulink environment, by using the Magic Formula and a set of scaling factors λ (where the default value of these factors is set equal to 1), the lateral forces F_y are so computed as a function of:

- slip angle α
- vertical forces F_z
- longitudinal slip of the tire (set equal to zero, since we are not considering the longitudinal dynamic of the vehicle)
- camber angle (set equal to zero)
- friction coefficient μ (equal in x and y direction)

3.4.2 Jacking forces

During cornering, the lateral forces exerted by the tires are transmitted to the body through the suspension links in order to guarantee the lateral force balance of the latter. As mentioned before, the suspension system can only transmit forces to the body along the vector passing through the tire contact patch, A_i, and the instantaneous centre of rotation of the suspension, J_i.

Figure 10 shows that during cornering, in order to generate a lateral force $F_{y,i}$, each suspension link have to generate a total force of modulus $F_{tire,i} = \frac{F_{y,i}}{\cos(\theta_i}$ with the same direction of the link itself.

As a consequence, the suspension system generates a vertical force $F_{Jack,i} = F_{tire,i} \sin(\theta_i \ = F_{y,i} tg(\theta_i$, which are known as Jacking forces.

Thus, in order to compute the forces transmitted through the suspensions to the body it is necessary to have: 1) a tire model to describe the lateral reaction of the tires as a function of the state variables of the system; 2) the values of the angles θ_i to compute the values of the Jacking forces.

Assuming that the length of suspension links in Figure 10 remains constant during small oscillation around the linearisation point, it is possible to compute the inclination of the link as it follows:

$$tg(\theta_i \ = \frac{Z_{J,i}}{\sqrt{l_{link,i}^2 - Z_{J,i}^2}} \tag{104}$$

where $Z_{J,i}$ is the height of the point J_i, which can be computed following the procedure described in section 0; $l_{link,i}$ is the length $\overline{TJ}_i$ of the i-th link relative to the i-th tire in the linearisation point.

It is possible to compute also the front and rear track width with trivial geometrical consideration:

$$\begin{aligned} t_F &= \left(\sqrt{l_{link,1}^2 - Z_{J,1}^2} + Y_{J,1}\right) + \left(\sqrt{l_{link,2}^2 - Z_{J,2}^2} - Y_{J,2}\right) \\ t_R &= \left(\sqrt{l_{link,4}^2 - Z_{J,4}^2} + Y_{J,4}\right) + \left(\sqrt{l_{link,3}^2 - Z_{J,3}^2} - Y_{J,3}\right) \end{aligned} \tag{105}$$

3.4.3 Vertical forces

The vertical load exerted on the tire is given by: the static load, the force generated by suspension, anti-roll bars and actuator, and the Jacking forces:

$$\begin{aligned} F_{z,1} &= \frac{mg}{2}\frac{b}{L} - (K_1 \Delta Z_{A,1} + C_1 \dot{Z}_{A,1})_{susp} + \frac{K_{t,F}}{t_F}\varphi + F_{y,1} tg(\theta_1 \ + F_{Act,1} \\ F_{z,2} &= \frac{mg}{2}\frac{b}{L} - (K_2 \Delta Z_{A,2} + C_2 \dot{Z}_{A,2})_{susp} - \frac{K_{t,F}}{t_F}\varphi - F_{y,2} tg(\theta_2 \ + F_{Act,2} \\ F_{z,3} &= \frac{mg}{2}\frac{a}{L} - (K_3 \Delta Z_{A,3} + C_3 \dot{Z}_{A,3})_{susp} - \frac{K_{t,R}}{t_R}\varphi - F_{y,3} tg(\theta_3 \ + F_{Act,3} \\ F_{z,4} &= \frac{mg}{2}\frac{a}{L} - (K_4 \Delta Z_{A,4} + C_4 \dot{Z}_{A,4})_{susp} + \frac{K_{t,R}}{t_R}\varphi + F_{y,4} tg(\theta_4 \ + F_{Act,4} \end{aligned} \tag{106}$$

Where $\Delta Z_{A_i} = Z_{A_i} - Z_{static,A_i}$ in which $Z_{A,i}$, as for $\dot{Z}_{A,i}$, is computed with (80); $F_{y,i}tg(\theta_i$ are the Jacking forces and $F_{Act,i}$ are the forces exerted by the actuators; $K_{t,F}$ and $K_{t,R}$ are the front and rear anti-roll bars stiffness; t_F and t_R are the front and rear track width expressed by (105); and φ is the roll angle.

3.4.4 Slip angles

The slip angles at the wheels can be computed as it follows:

$$\alpha_i = \beta_i - \delta_i \tag{107}$$

Where β_i and δ_i are, respectively, the side slip angle and the steering angle of the i-th wheel.
The steering angle in this case is considered to be equal for the front wheels, while is zero for the rear ones.

The side slip angle β_i is computed by dividing the lateral speed of the tire for its longitudinal speed, thus obtaining:

$$\alpha_i = \frac{\dot{y}^*_{T_i}}{\dot{x}^*_{T_i}} - \delta_i \tag{108}$$

The lateral and longitudinal speeds of the i-th tire have to be obtained in the intermediate frame and as function of the generalised coordinates, so we start by computing the position of the i-th tire expressed in the intermediate reference frame as a function of the generalised coordinates:

$$\{T'_1\} = \begin{Bmatrix} a \\ y^*_{J_1} - \dfrac{Z_{J_1}}{tg(\theta_1} \\ 0 \end{Bmatrix} \qquad \{T'_2\} = \begin{Bmatrix} a \\ y^*_{J_2} + \dfrac{Z_{J_2}}{tg(\theta_2} \\ 0 \end{Bmatrix} \tag{109}$$

$$\{T_3'\} = \begin{Bmatrix} -b \\ y^*_{J_3} + \dfrac{Z_{J_3}}{tg(\theta_3} \\ 0 \end{Bmatrix} \quad \{T_4'\} = \begin{Bmatrix} -b \\ y^*_{J_4} - \dfrac{Z_{J_4}}{tg(\theta_4} \\ 0 \end{Bmatrix}$$

Where:

$$\begin{Bmatrix} x^*_{J_i} \\ y^*_{J_i} \\ Z_{J_i} \end{Bmatrix}_{J_i} = R_{yx} \bullet \{J_i\} \tag{110}$$

At this point the speed vector for each tire is computed as following:

$$\{\dot{T}\}_i = R_{yx} \bullet \begin{Bmatrix} v_x \\ v_y \\ v_z \end{Bmatrix} + S_z \bullet \{T_i'\} + \{\dot{T}_i'\} \tag{111}$$

Where the speed along z in then assumed to be zero, the vector $\{v_x \ v_y \ v_z\}^T$ contains the speeds of the vehicle centre of mass respect to the body reference frame.

S_z can be written as:

$$S_z = \begin{bmatrix} 0 & -\dot{\psi} & 0 \\ \dot{\psi} & 0 & 0 \\ 0 & 0 & 0 \end{bmatrix} \tag{112}$$

The yaw rate $\dot{\psi}$ is finally rewritten as a function of the quasi-velocities by means of (52), thus obtaining:

$$\dot{\psi} = \Omega_y \cdot \varphi + \Omega_z \tag{113}$$

3.5 Simulink implementation

After all the dynamic equation of the system have been obtained following the previous analytical procedure, they need to be implemented in Matlab/Simulink environment in order to simulate the time response of the vehicle when subject to certain inputs. To do so it's possible to export the equations computed in Maple as Matlab file, and then use them to create the Simulink model.

In this first implementation of the model the longitudinal dynamics have been completely neglected and the longitudinal speed of the vehicle is fixed. By doing this we introduce some approximations, but at the same time the model is easier to implement and enough reliable for our purpose.
Given that the longitudinal dynamics are neglected, we do not consider the motor/braking torque at the wheels and the only inputs of our system are the steering angle and the front-to-total anti-roll moment distribution f. Inside the equations of motion, the position of the J_i point is considered as a known variable of the system, so we need to know the position of those points in order to properly define the system. The definition of the J_i point position is crucial to properly model the kinematic of the suspensions as it depends from the particular suspension system of the vehicle, and it can heavily affect the behaviour of the latter.

3.5.1 Computation of the J-points position

It is possible, knowing the particular geometry of the suspension used in the vehicle, to compute geometrically the position of the instantaneous centre of rotation of the suspension, that correspond to our J_i. Thus, after the suspension geometry is defined is possible to generate one look-up table for each suspension which, depending from the position of the vehicle, return the instantaneous position of the i-th J point. In this study the position of the J-points is computed by using 2D lookup tables, and the inputs of those are:

- roll angle φ
- vertical displacement of the front Z_{front} and the rear Z_{rear} of the vehicle as a function of the pitch angle θ and the semi-wheelbase a (front), b(rear) as it follows:

$$Z_{front} = Z - a \cdot \tan\theta \tag{114}$$

$$Z_{rear} = Z + b \cdot \tan\theta \tag{115}$$

Two lookup tables are so implemented for each suspension, one for the definition of the lateral displacement along the y-axis (l_J) and one for the vertical displacement along the z-axis (h_J). This set of coordinates identify the position of the J-points in the intermediate reference frame.

Thus, following the above procedure the position of the T-point along y-axis (T_J) is computed then in the intermediate reference frame.

The length of the four links are thus computed with the following formulation:

$$l_{link} = \sqrt{(T\_y - l\_J\ ^2 + h\_J^2} \tag{116}$$

3.5.2 Non-linear model

The non-linear equations of motion of the system are thus implemented in Simulink by means of Matlab function in which the inputs are the variables on the right side of the equation while the output is the variable on the left side of the equation (if the block contains a system of equation we can have multiple outputs). The Simulink model is divided in five different subsystem: four of them contain the equation of motion computed previously and the equations to compute the forces acting on the body of the vehicle, the fifth instead presents a simple controller to compute the active forces generated by the actuators on each suspension as function of the lateral acceleration of the vehicle (Figure 12).

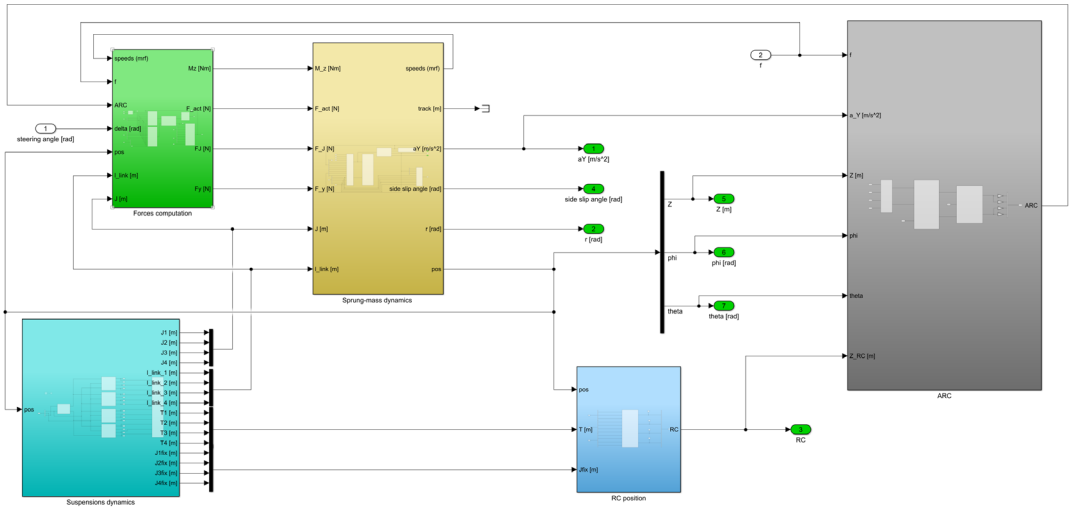

Figure 12. Simulink non-linear model: subsystems

More specifically, the model is divided in the following subsystems:

- Sprung-mass dynamics (yellow): it contains the equation of motion of the vehicle; the inputs are the forces acting on the body and the positions of the J points.

- Forces computation (green): it contains the equation to compute the vertical, lateral and jacking forces generated by the contact between the tires and the ground; the inputs are the states of the vehicle, the steering angle, the value of f, and the positions of the J points.
- Suspension dynamics (turquoise): it contains the lookup-tables that give us the position of the J points; the inputs are the states of the vehicle.
- RC position (blue): it computes the position of the two roll centres (front and rear) knowing the position of the J points and the contact patches of the tires.
- ARC (grey): it computes the force of the actuators; the inputs are the states of the system, the positions of the RCs and the lateral acceleration of the vehicle.

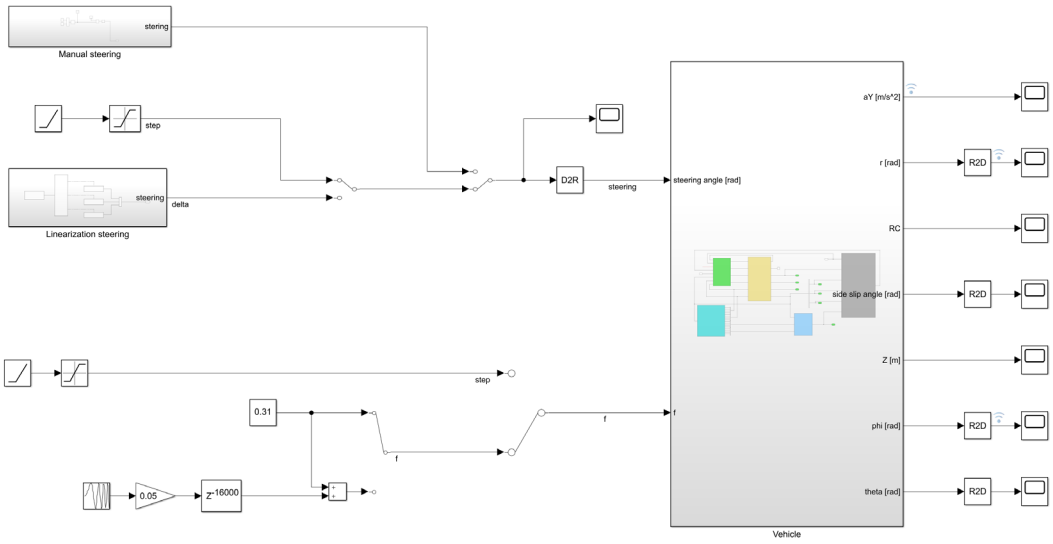

Figure 13. Simulink non-linear model: main system

All the subsystems are then grouped in a single system (Figure 13) in which the only inputs are the steering angle and the value f, while the outputs are: the lateral acceleration a_Y, the yaw rate r, the RCs positions, the side slip angle β, the height of the centre of gravity Z, the roll angle φ, the pitch angle θ. Using this model is possible to perform simulation in the time domain of all kind of manoeuvres by generating the desired steering input (ramp, step, sine, sine with dwell).

3.5.3 Model linearisation

In order to obtain a linear model, it is possible to use the linear analysis tool built in Simulink, which allows to linearize a single block of the model, in a specific linearization point, obtaining the state space formulation in which the inputs and outputs correspond to the ones of the linearized block.

In this case the subsystem *Vehicle* simulate (Figure 13) the vehicle dynamics and the inputs are the steering angle and the front-to-total anti-roll moment ratio.

In order to linearise the system we need to properly define the linearisation point which has to be an equilibrium point of the system of differential equations. For this reason, the system has been linearised for $t = 25$ s when subject to the steering input in Figure 14a and a value of anti-roll moment $f = 0.5$.

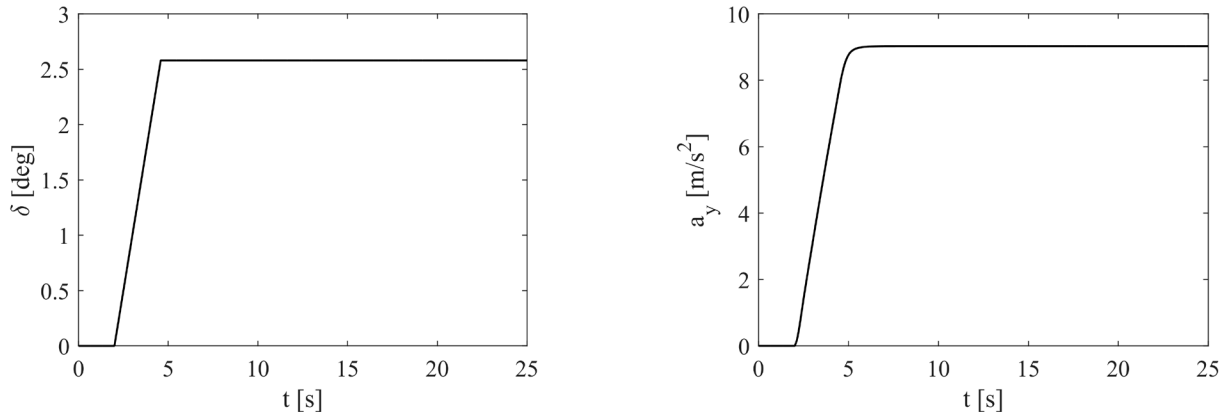

Figure 14. a) steering angle during linearisation versus time b) lateral acceleration during linearisation versus time

At this point the vehicle model is in static conditions (Figure 14b shows that the value of lateral acceleration remains stable at 9 m/s^2), subject to a lateral acceleration of 9 m/s^2 and a longitudinal speed of 100 km/h, which in this case are defining our linearisation point.

At this point, by means of the linear analysis tool, the linearised system is obtained in state space form.

3.6 Results

In the following sections two types of analysis are carried out in order to verify the response of the newly developed model. In the first part the time response of the passive vehicle (i.e. when the active part of the

suspensions is deactivated) will be analysed, while in the second one the effect of the active suspension system will be analysed looking at the frequency response of the active vehicle.
In both cases the simulation will be carried out in two cases:

- With fixed RCs positions: The Roll Centres lie on the ground and they are fixed respect to the vehicle body and the intermediate reference frame, thus the suspensions kinematic are neglected. By doing this we introduce the same simplifications used in the previous model, so we expect similar results from the two models and this can be used to verify if the new model works properly.
- With moving RCs: The positions of the roll centres depend on the suspension kinematics, thus they vary according to the movements of the vehicle body. These simulations can be carried out only with the newly developed model, and these will be used to analyse the effect of the Roll Centres migration on the forces acting on the vehicle and its frequency response (for the active case)

In the following sections these analyses will be carried out, and they can be summarised as it follows:

1. Passive case with fixed RCs (time domain comparison: old model vs. new model)
2. Passive case with moving RCs (time domain analysis: effects of Roll Centre migration)
3. Active case with fixed RCs (frequency domain comparison: old model vs. new model)
4. Active case with moving RCs (frequency domain analysis: effects of Roll Centre migration)

3.6.1 Passive case with fixed RCs: ramp steer manoeuvre simulation (passive vehicle)

In order to compare the new model with the validated model, a ramp steer manoeuvre has been simulated. The simulation is carried out at a constant speed $V_0 = 100$ km/h with the steering inputs shown in Figure 15. In the validated vehicle model, the roll centre is considered as a fixed point which lies on the ground for both axles, thus we need to impose the same simplification also to the new one in order to properly compare the two models. For this reason, at this stage, the J points are considered as fixed points that are lying on the ground, therefore the roll centre is fixed and lies on the ground as well. Under this

assumption, the results obtained by performing the same manoeuvre with both models are reported in Figure 16. The results obtained by performing a ramp steer manoeuvre show that the two models

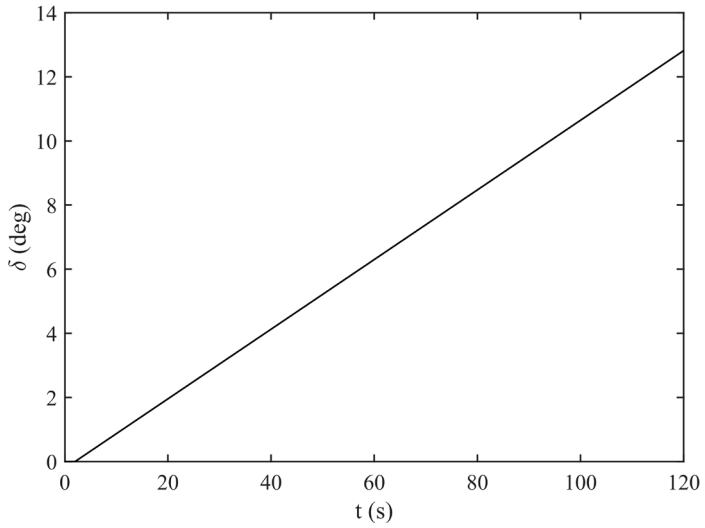

Figure 15. Steering angle during ramp steer

behaviour is very similar, whit some difference only for high values of lateral acceleration Both models show a discontinuity in the lateral acceleration and the yaw rate for $t \cong 50$ s, which corresponds to the instant in which the vertical load on the inner front tire of the vehicle goes to zero.

Given the good match between the two simulations, the newly developed model can be considered a reliable model for vehicle dynamics simulations.

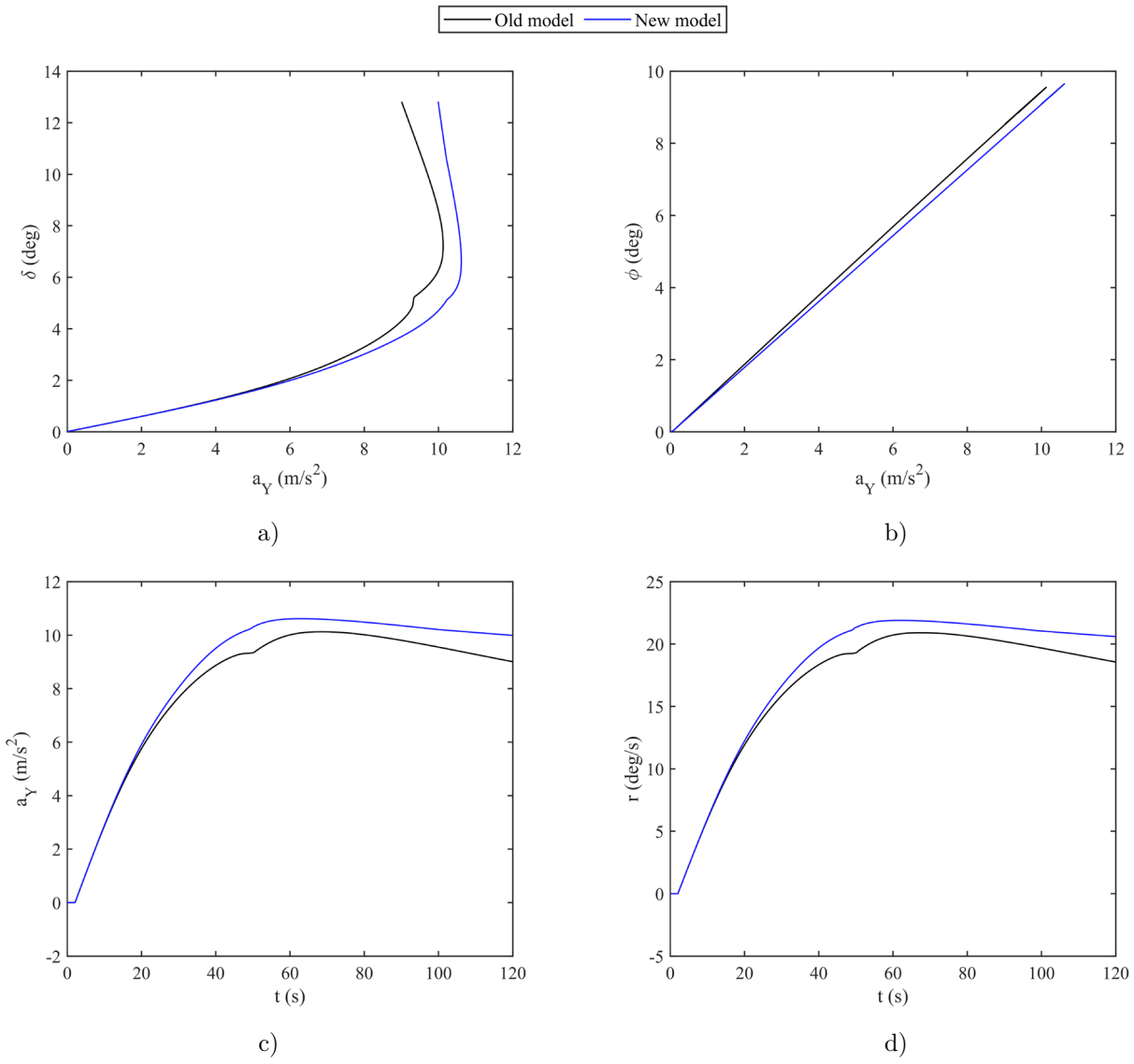

Figure 16. Passive vehicle results: a) steering angle vs. lateral acceleration b) roll angle vs. lateral acceleration c) lateral acceleration vs. time d) yaw rate vs. time

3.6.2 Passive case with moving RCs: effect of Roll Centre migration on the Jacking forces

In this section presents an analysis on the effect of the roll centre migration on the Jacking forces, the heave and the roll gain of the vehicle. By using the new model, it is possible to modify the suspension kinematics (by modifying the lookup-tables of the J-points), thus obtaining different behaviour of the roll centre simulating the same manoeuvre. In this case the analysis is carried out by simulating a step steer manoeuvre with a slope of 1 deg/s and a maximum value of $\delta = 2.0$ deg, and by considering four different cases of roll centre migration. This has been done to reproduce the results reported in [16] by the author

Gerrard M.B., and then to compare them to the ones obtained in the real case by considering the lateral load transfer. In Figure 17 reports the results of the simulations.

Figure 17a shows the four cases of roll centre migration for which the analysis has been carried out: the axis reported in the figure correspond to the ones of the intermediate reference frame of the vehicle, and the inner side of the corner in this case correspond to the one with positive values of Y.

The dashed lines have been obtained by disabling the lateral load transfer in the model, and thus they should reproduce the results discussed in [16]. When the lateral forces generated by the two wheels of the same axle are the same, according to *Gerrard M.B.,* we should expect the following results:

- RC above the ground level and toward the inner side of the corner (1^{st} quadrant):

  The total Jacking force of the axles are negative, thus the body of the vehicle falls during cornering.

- RC above the ground level and toward the outer side of the corner (2^{nd} quadrant):

  The total Jacking force of the axles are positive, thus the body of the vehicle rises during cornering.

- RC under the ground level and toward the inner side of the corner (3^{rd} quadrant):

  The total Jacking force of the axles are negative, thus the body of the vehicle falls during cornering.

- RC under the ground level and toward the outer side of the corner (4^{th} quadrant):

  The total Jacking force of the axles are positive, thus the body of the vehicle rises during cornering.

Looking at the dashed lines in Figure 17 it is possible to see that the results obtained through simulations confirm what said in [16], but under real conditions the lateral forces generated by the wheels of the same axle can be quite different, thus this results are no more valid. In fact, looking at the solid lines, the results obtained considering the lateral load transfer can be significantly different, and in some cases even opposite such in the case where the Roll Centre moves toward the inner side of the corner above the ground (blue line, 1^{st} quadrant).

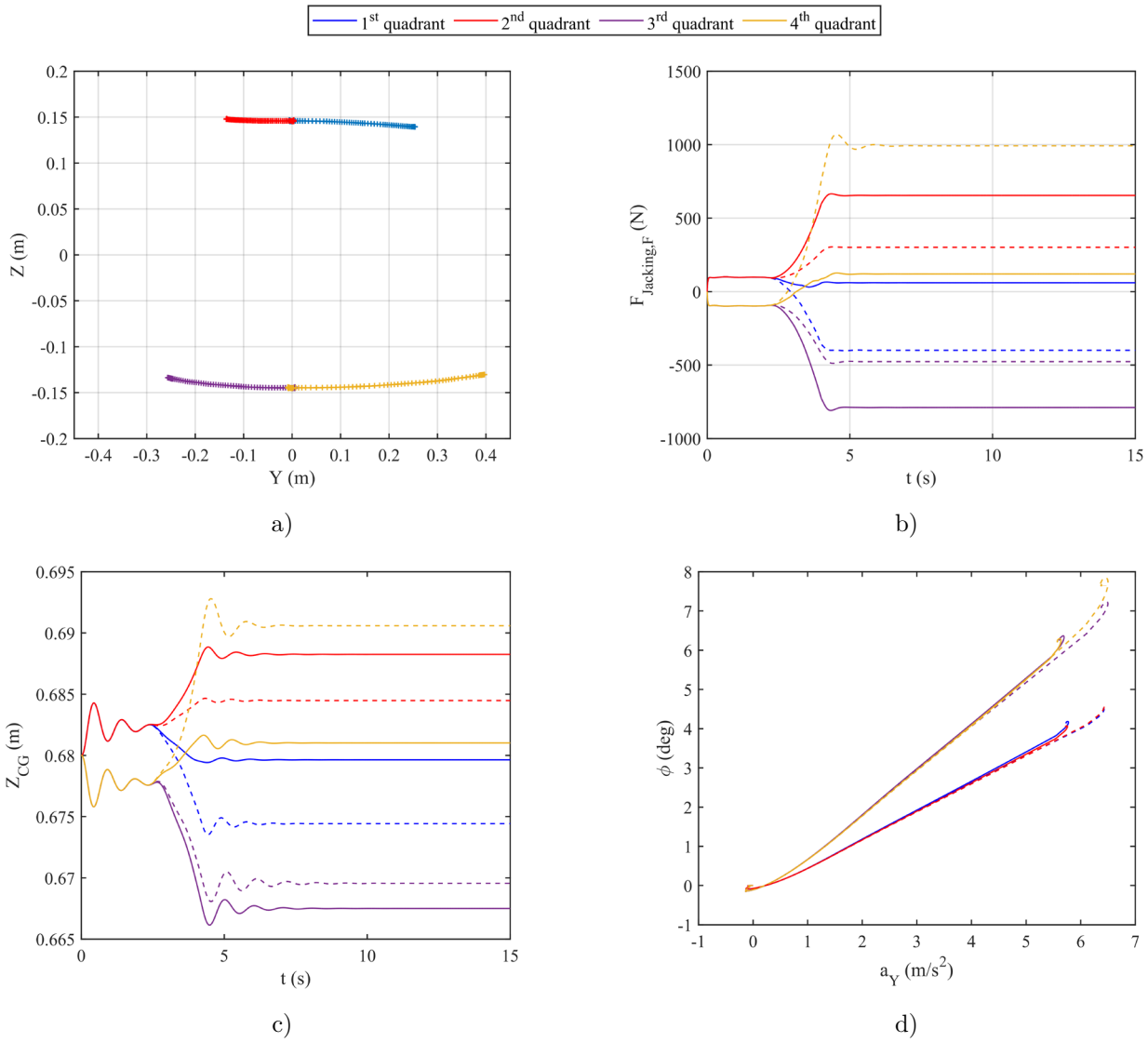

Figure 17. Roll Centre migration comparison: a) Locus of the front roll centre b) front axle Jacking forces vs. time c) Height of the centre of gravity of the vehicle vs. time d) Roll angle vs. lateral acceleration. The figure reports two cases: the dashed lines have been obtained without lateral load transfer, while the solid lines have been obtained considering the lateral load transfer

In that case, according to [16], we should have negative Jacking forces and the body of the vehicle that falls during cornering, while if we consider the lateral load transfer the Jacking force of the front axle becomes negligible and therefore also the vertical movement of the vehicle body. This means that it is not possible to predict the direction and the amplitude of the Jacking forces, and consequently of the vertical motion of the vehicle, without knowing the specific parameters and tires of the vehicle, because these forces are strongly influenced by the latter and the results can differ significantly.

Finally, Figure 17d shows that the lateral migration of the roll centre do not have a big impact on the roll gain of the vehicle, while the vertical movement of the roll centre can heavily affect the roll characteristic of the vehicle.

3.6.3 Active case with fixed RCs: frequency response comparison

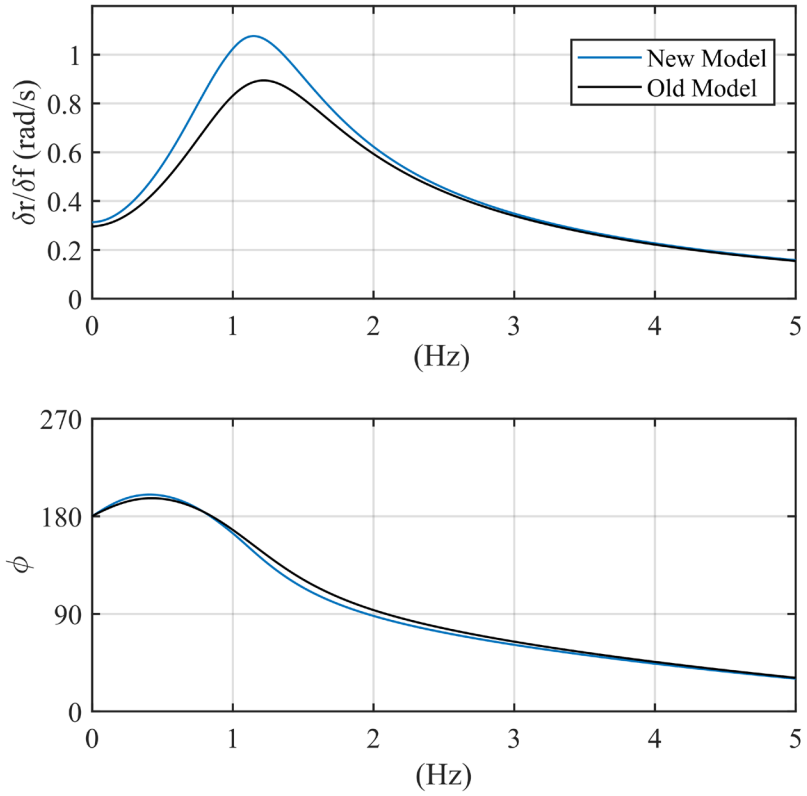

Figure 18. Bode plot of $\delta r/\delta f$ at 100 km/h under a lateral acceleration $a_Y = 9\ m/s^2$ and $f_0 = 0.5$

By using the state space form of the system, it is possible to carry out different analysis, one of which is the analysis in the frequency domain of the yaw rate (δr) response to a variation of front-to-total anti-roll moment variation (δf). Figure 18 reports the bode plot of the transfer function $\delta r/\delta f$ of the system, which shows a resonance around a frequency of 1.2 Hz. Except some difference in the magnitude of the resonance peak, the two bode plots show very similar magnitude and phase, and thus also for the active case we can consider the new model a reliable model also for frequency analysis purpose.

The new model is therefore suitable for a model-base design approach to develop controller for different kind of active systems as anti-roll moment distribution control, dynamic lift, pitch control and so on.

3.6.4 Active case with moving RCs: frequency response analysis for different RC positions

Figure 19 and Figure 20 report the result of the frequency response analysis carried out with the active suspension enabled and considering the roll centre migration. The plots show the results obtained with five different position of the roll centre: the four coloured lines have been obtained considering the roll centre migration in the four quadrants (as in Figure 17a), while the black line has been obtained with the new model considering the roll centre fixed on the ground (as in the previous section).

Looking at Figure 19 it is clear that the lateral migration of the roll centre do not have a big influence on the yaw rate frequency response, while the vertical displacement of RC has a strong impact on the magnitude of latter. In fact, the two lines obtained with the RC above the ground (blue and red) are really similar and the same applies to the results obtained the RC is under the ground level (violet and yellow), but the farther away the RC gets from the vehicle centre of gravity, the bigger the magnitude of the frequency response becomes. In this case the centre of gravity of the vehicle is around $Z_{CG} \cong 0.68$ m, thus we obtain the higher magnitude of the frequency response when the RC is under the ground, while we the smallest one is obtained when the latter is above the ground level. The reason why this happens is to be found in the variation of the arm of the inertia forces, and therefore in the roll moment generated by the latter.

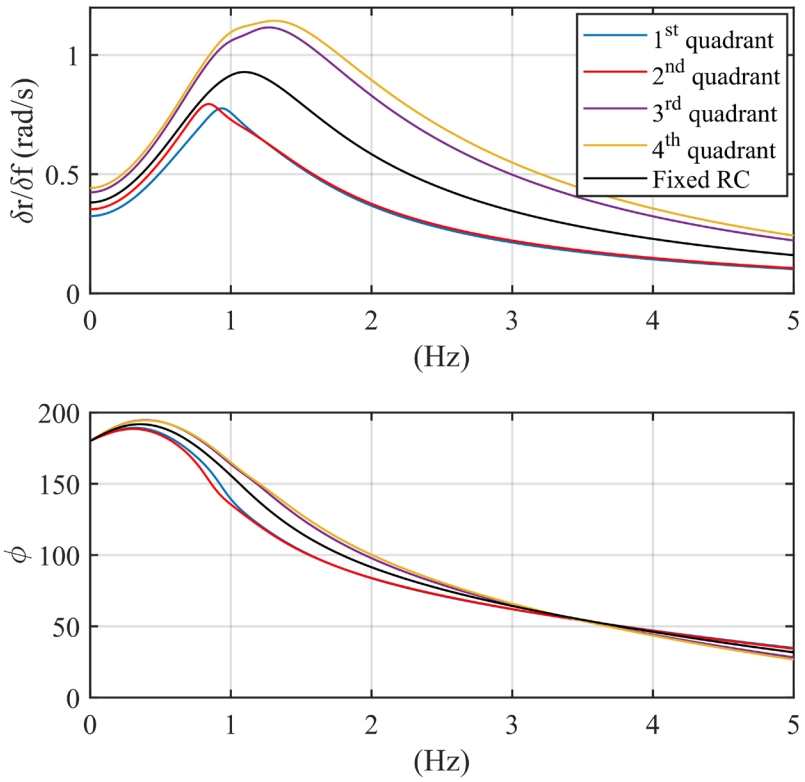

Figure 19. Frequency response of the yaw rate of the vehicle to a variation of the anti-roll moment distribution, $\delta r/\delta f$, when linearised for a longitudinal speed $V_0 = 100\ km/h$, a lateral acceleration of $a_y = 9\ m/s^2$ and $f_0 = 0.5$.

By increasing this quantity, we increase also the active anti-roll moment generated by the actuators (because the anti-roll controller tries to maintain the same roll angle), and thus the same variation of f will generate a bigger variation of anti-roll moment transferred from one axle to the other.

This leads to a strong variation of lateral forces generated by the axles, and consequently to the behaviour described above. In this case the phase of the frequency response is almost equal in all five cases.

Differently from the previous case, the frequency response $\delta Z_{CG}/\delta f$ show some sensibility also to the lateral migration of the roll centre. This is due to the fact that the main responsible for the variation of the height of the centre of gravity are the Jacking forces. As seen in Figure 17b, these forces are heavily affected by the movement of the roll centre, and this translates to the results obtained in Figure 20.

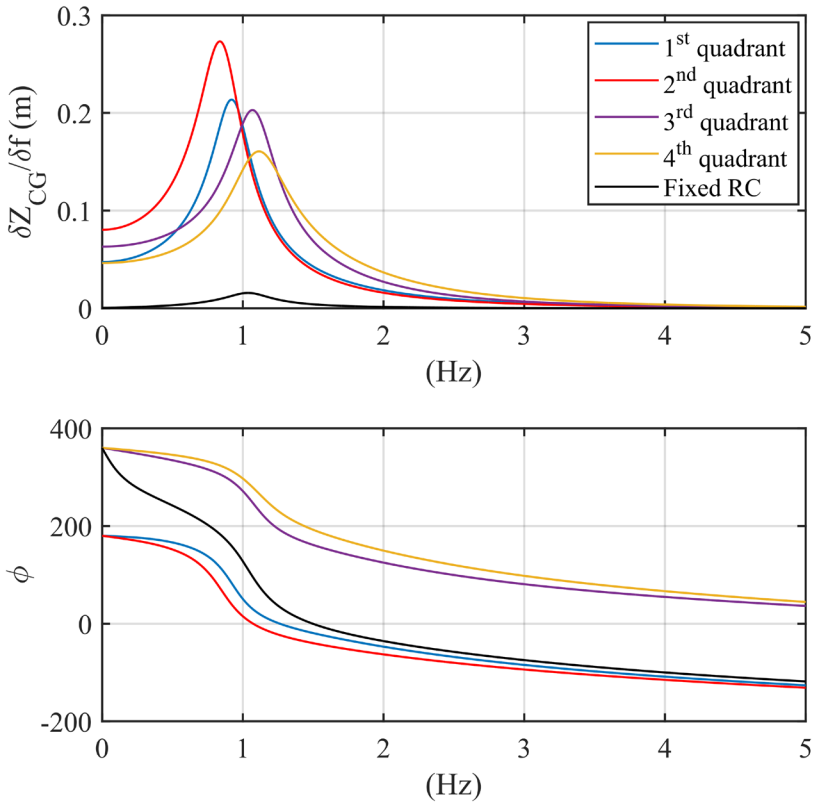

Figure 20. Frequency response of the height of the vehicle centre of gravity to a variation of the anti-roll moment distribution, $\delta Z_{CG}/\delta f$, when linearised for a longitudinal speed $V_0 = 100\ km/h$, a lateral acceleration of $a_y = 9\ m/s^2$ and $f_0 = 0.5$.

The black line, representing the case in which the Roll centre lies to the ground, shows almost zero magnitude because in this condition the forces generated by the tires are parallel to the ground, thus the Jacking forces are equal to zero. Opposite to the previous case, when the roll centre is above the ground we obtain higher magnitude in the frequency response of Z_{CG} to f. Moreover, the frequency response shows other two differences:

1. The magnitude of the frequency response results higher when the roll centre moves towards the outside of the corner.

2. The static phase of the response is 360 degrees when the roll centre is below the ground while is 180 degrees when the roll centre is above the ground.

In order to properly explain this behaviour, it is convenient to look at the Jacking forces generated when the vehicle is subject to the same acceleration in which the system has been linearised. Figure 21 show

the results obtained by simulating a step steer manoeuvre with a slope of 1 deg/s and a maximum steering angle $\delta = 2.51$ deg, to which correspond a lateral acceleration $a_y = 9$ m/s.

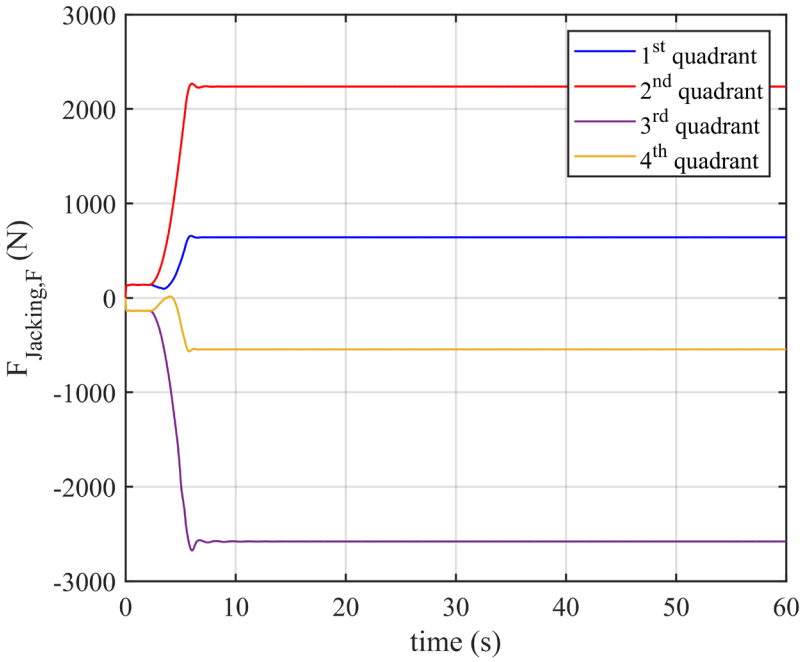

Figure 21. Front axle Jacking force for a lateral acceleration $a_y = 9\ m/s^2$

The first difference can be explained by looking at Figure 21, which shows that when the roll centre moves toward the outside of the corner the Jacking forces generated are much higher than those obtained with the roll centre moving towards the inside of the corner. This means that the same variation of f has more influence in the first case because it involves a bigger variation of Jacking forces.

The phase difference, instead, is due to the sign of the Jacking forces, which is positive when the RC is above the ground (blue and red lines) and negative in the other cases. This means that an increase of the magnitude of the Jacking force has the opposite effect on the vertical movement of the vehicle body, and thus we obtain opposite phases in the frequency response.

4 Conclusions

In this thesis a model-based design procedure for the synthesis of an active suspension controller has been discussed, and the controller thus obtained has been tested in simulation by means of a validated vehicle model in MATLAB/Simulink environment. The results of this analysis show that: by using an active suspension system to actively control the yaw rate of the vehicle it is possible to increase the both performance and safety when the vehicle is under limit conditions. Then, a novel vehicle model, which can be used in a model-base design approach, has been developed. The new model takes into account 6 degrees of freedom for the body of the vehicle, the suspension kinematics and an actuator for each one of the four suspensions, in order to simulate different active systems. The equation of motion of the vehicle have been computed analytically and then they have been implemented in MATLAB/Simulink. Once created, it has been linearised by means of the linear analysis tool built in Simulink and thus the linearised model has been obtained in state space form.

Therefore, different analyses have been carried out, in the first place to verify that the new model was behaving correctly, and then to study the influence of the roll centre migration on the vehicle behaviour. The results showed that the model was reliable for both simulation and linearisation purpose, and that the migration of the roll centre can have a strong influence mainly on the vertical and roll dynamics of the vehicle. Therefore, the roll centre migration has to be taken into account to have a better representation of the vehicle behaviour, and this is especially true when we are interested in the study of vertical and roll dynamics.

5 Bibliography

[1] Y. Furukawa and M. Abe, "Advanced Chassis Control Systems for Vehicle Handling and Active Safety," *Vehicle System Dynamics,* vol. 28, no. 2-3, pp. 59-86, 1997.

[2] Y. Jialing, R. Shan, L. Zhihong and T. Saied, "Improving lateral stability by distributing roll moment via semi-active suspension," *FISITA World Automotive Congress,* 2016.

[3] D. Williams and W. Haddad, "Nonlinear control of roll moment distribution to influence vehicle yaw characteristics," *IEEE Trans. on Control Systems Technology,* vol. 3, no. 1, p. 110–116, 1995.

[4] J. Wang, D. Wilson, W. Xu and D. Crolla, "Active suspension control to improve vehicle ride and steady-state handling," *Proceedings of the 44th IEE Conference on Decision and Control,* p. 1982–1987, 2005.

[5] T. Chu and R. P. Jones, "Analysis and simulation of nonlinear handling characteristics of automotive vehicles with focus on lateral load transfer," *Vehicle System Dynamics,* vol. 46, no. 1, pp. 17-31, 2008.

[6] M. Bodie and A. Hac, "Closed loop yaw control of vehicles using magneto-rheological dampers," *SAE Technical Paper,* Vols. 2000-01-0107, 2000.

[7] B. Badji, E. Fenaux, M. E. Bagdouri and A. Miraoui, "Nonlinear single track model analysis using Volterra series approach," *International J. of Vehicle Design,* vol. 47, no. 1, pp. 81-98, 2009.

[8] H. B. Pacejka, "Tire and vehicle dynamics," *Elsevier,* 2005.

[9] M. Lakehal-Ayat and E. F. S. Diop, "An improved active suspension yaw rate control," *In Proceedings of the 2002 American Control Conference (IEEE Cat. No. CH37301),* vol. 2, pp. 863-868, 2002.

[10] W. Cho, J. Choi, C. Kim, S. Choi and K. Yi, "Unified chassis control for the improvement of agility, maneuverability, and lateral stability," *IEEE Transactions on vehicular Technology,* vol. 61, no. 3, pp. 1008-1020, 2012.

[11] M. Shin, S. Bae, J. M. Lee, J. Lee, S. Heo and T. O. Tak, "New vehicle dynamics model for yaw rate estimation," *Vehicle System Dynamics,* vol. 37, pp. 96-106, 2002.

[12] C. Chatzikomis, A. Sorniotti, P. Gruber, M. Bastin, R. M. Shah and Y. Orlov, "Torque-vectoring control for an autonomous and driverless electric racing vehicle with multiple motors," *SAE International Journal of Vehicle Dynamics, Stability, and NVH,* vol. 1, no. 2, pp. 338-351, 2017.

[13] L. De Novellis, A. Sorniotti and P. Gruber, "Optimal wheel torque distribution for a four-wheel-drive fully electric vehicle," *SAE International Journal of Passenger Cars-Mechanical Systems,* vol. 6, no. 1, pp. 128-136, 2013.

[14] I. P. S. Skogestad, Multivariable feedback control: analysis and design, Wiley, 2007.

[15] G. Genta and L. Morello, The automotive chassis: volume 2: system design, Springer Science & Business Media, 2008.

[16] M. B. Gerrard, "Roll Centres and Jacking Forces in Independent Suspensions-A First Principles Explanation and a Designer's Toolkit," *SAE Technical Paper,* no. No. 1999-01-0046, 1999.

[17] M. Yamamoto, "Active Control Strategy for Improved Handling and Stability," *SAE transaction,* vol. 100, no. 6, p. 16381648, 1991.

[18] G. Genta, Motor vehicle dynamics: modeling and simulation, World Scientific, 1997.

[19] M. Abe, "A study on effects of roll moment distribution control in active suspension on improvement of limit performance of vehicle handling," *Int. J. of Vehicle Design,* vol. 15, no. 3-5, pp. 326-336, 1994.

[20] A. Thompson, "An active suspension with optimal linear state feedback," *Vehicle Systems Dynamics,* vol. 5, no. 4, pp. 187-203, 1976.

[21] A. Al-Zughaibi and H. Davies, "Controller design for active suspension system of ¼ car with unknown mass and time delay," *International Journal of Mechanics and Mechatronics Engineering,* vol. 9, no. 8, pp. 1484-1489, 2015.

[22] A. Zaremba, R. Hampo and D. Hrovat, "Optimal active suspension design using constrained optimization," *Journal of Sound and Vibration,* vol. 207, no. 3, pp. 351-364, 1997.

[23] A. Baumal, J. McPhee and P. Calamai, "Application of genetic algorithms to the design optimization of an active vwhicle suspension system," *Computer Methods in Applied Mechanics and Engineering,* vol. 163, no. 1-4, pp. 87-94, 1998.

[24] B. Lenzo, A. Sorniotti, P. Gruber and K. Sannen, "On the experimental analysis of single input single output control of yaw rate and sideslip angle," *Int. J. of Automotive Technology,* vol. 18, no. 5, pp. 799-811, 2017.

[25] C. Chatzikomis, A. Sorniotti, P. Gruber, M. Bastin, R. M. Shah and Y. Orlov, "Torque-vectoring control for an autonomous and driverless electric racing vehicle with multiple motors," *SAE International Journal of Vehicle Dynamics,* vol. 1, no. 2, pp. 338-351, 2017.

[26] D. Danesin, P. Krief, A. Sorniotti and M. Velardocchia, "Active roll control to increase handling and comfort," *SAE transactions,* pp. 1007-1017, 2003.

[27] E. Elbeheiry, Y. Zeyada and M. Elaraby, "Handling Capabilities of Vehicles in Emergencies Using Coordinated AFS and ARMC Systems," *Vehicle System Dynamics,* vol. 35, no. 3, pp. 195-215, 2001.

[28] F. Hasbullah, F. D. W. Faris and M. Abdelrahman, "Ride comfort performance of a vehicle using active suspension system with active disturbance rejection control," *International Journal of Vehicle Noise and Vibration,* vol. 11, no. 1, pp. 78-101, 2015.

[29] I. Fialho and G. Balas, "Road adaptive active suspension design using linear parameter-varying gain-scheduling," *IEEE Transactions on Control Systems Technology,* vol. 10, no. 1, pp. 43-54, 2002.

[30] H. Heo, E. Joa, K. Yi and K. Kim, "Integrated chassis control for enhancement of high speed cornering perfomance," *SAE Int. J. Commer. Veh,* pp. 102-109, 2015.

[31] J. Gerhard, M. Laiou, M. Monnigmann and W. Marquardt, "Robust yaw control design with active differential and active roll control systems," *IFAC Proceedings,* vol. 38, no. 1, pp. 73-78, 2005.

[32] H. Her, J. Suh and K. Yi, "Integrated control of the differential braking, the suspension damping force and the active roll moment for improvement in the agility and the stability," *J. Automobile Engineering,* vol. 229, no. 9, pp. 1145-1157, 2015.

[33] P. Michelberg, L. Palkovisc and J. Bokor, "Robust design of active suspension system," *International Journal of Vehicle Design,* vol. 14, no. 2-3, pp. 145-165, 1993.

[34] N. Cooper, D. Crolla and M. Levesley, "Integration of active suspension and active driveline to ensure stability while improving vehicle dynamics," *SAE Technical Paper,* Vols. 2005-01-0414, 2005.

[35] M. Coric, J. Deur, J. Kasak and H. Tseng, "Optimisation of active suspension control inputs for improved vehicle handling performance," *Vehicle System Dynamics,* vol. 54, no. 11, pp. 1574-1600, 2016.

[36] F. Yu and D. Crolla, "An optimal self –tuning controller for an active suspension," *Vehicle Systems Dynamics,* vol. 29, no. 1, pp. 51-65, 1998.

[37] T. Shim and D. Margolis, "Dynamic normal force control for vehicle stability enhancement," *International journal of vehicle autonomous systems,* vol. 3, no. 1, pp. 1-14, 2005.

[38] S. Varnhagen, O. Anubi, Z. Sabato and D. Margolis, "Active suspension for the control of planar vehicle dynamics," *IEEE International Conference on Systems, Man, and Cybernetics (SMC),* pp. 4085-4091, 2014.

[39] C. Clover and J. Bernard, "The Influence of Lateral Load Transfer Distribution on Directional Response," *SAE Technical Paper,* no. 930763, 1993.

[40] T. Xinpeng and D. Xiaocheng, "Simulation and study of active roll control for SUV based on fuzzy PID," *SAE Technical Paper,* Vols. 2007-01-3570, 2007.

[41] Y. Xu and M. Ahmadian, "Improving the capacity of tire normal force via variable stiffness and damping suspension system," *J. of Terramechanics,* vol. 50, no. 2, pp. 122-132, 2013.